

7-1-2020

CD4 Deficiency Causes Poliomyelitis and Axonal Blebbing in Murine Coronavirus-Induced Neuroinflammation.


Debanjana Chakravarty
Indian Institute of Science Education and Research

Fareeha Saadi
Indian Institute of Science Education and Research

Soumya Kundu
Indian Institute of Science Education and Research

Abhishek Bose
Indian Institute of Science Education and Research

Reas Khan
Follow this and additional works at: <https://jdc.jefferson.edu/pacbfp>
University of Pennsylvania Scheie Eye Institute

 Part of the [Cells Commons](#)

[Let us know how access to this document benefits you](#)

See next page for additional authors

Recommended Citation

Chakravarty, Debanjana; Saadi, Fareeha; Kundu, Soumya; Bose, Abhishek; Khan, Reas; Dine, Kimberly; Kenyon, Lawrence C; Shindler, Kenneth S; and Das Sarma, Jayasri, "CD4 Deficiency Causes Poliomyelitis and Axonal Blebbing in Murine Coronavirus-Induced Neuroinflammation." (2020). *Department of Pathology, Anatomy, and Cell Biology Faculty Papers*. Paper 299.
<https://jdc.jefferson.edu/pacbfp/299>

This Article is brought to you for free and open access by the Jefferson Digital Commons. The Jefferson Digital Commons is a service of Thomas Jefferson University's [Center for Teaching and Learning \(CTL\)](#). The Commons is a showcase for Jefferson books and journals, peer-reviewed scholarly publications, unique historical collections from the University archives, and teaching tools. The Jefferson Digital Commons allows researchers and interested readers anywhere in the world to learn about and keep up to date with Jefferson scholarship. This article has been accepted for inclusion in Department of Pathology, Anatomy, and Cell Biology Faculty Papers by an authorized administrator of the Jefferson Digital Commons. For more information, please contact: JeffersonDigitalCommons@jefferson.edu.

Authors

Debanjana Chakravarty, Fareeha Saadi, Soumya Kundu, Abhishek Bose, Reas Khan, Kimberly Dine, Lawrence C Kenyon, Kenneth S Shindler, and Jayasri Das Sarma

CD4 deficiency causes poliomyelitis and axonal blebbing in murine coronavirus induced neuroinflammation

Running title: CD4 T cells prevent poliomyelitis and axonal dystrophy

Debanjana Chakravarty^{1#}, Fareeha Saadi^{1#}, Soumya Kundu¹, Abhishek Bose¹, Reas Khan², Kimberly Dine², Lawrence C Kenyon³, Kenneth S Shindler^{2,4*} and Jayasri Das Sarma^{1,*}

¹Department of Biological Sciences, Indian Institute of Science Education and Research
Kolkata, Mohanpur-741246, India

²Departments of Ophthalmology and ⁴Neurology University of Pennsylvania Scheie Eye
Institute, Philadelphia, PA 19104, USA

³Department of Pathology, Anatomy and Cell Biology, Thomas Jefferson University,
Philadelphia, PA 19107, USA

ABSTRACT:

Mouse hepatitis virus (MHV) is a murine β -coronavirus (m-CoV) which causes a wide range of diseases in mouse and rat, including hepatitis, enteritis, respiratory diseases, and encephalomyelitis in the CNS. MHV infection in mice provides an efficient cause-effect experimental model to understand the mechanisms of direct virus induced neural cell damage leading to demyelination and axonal loss which are pathological features of Multiple sclerosis (MS), the most common disabling neurological disease in young adults. Infiltration of T lymphocytes, activation of microglia and their interplay are the primary pathophysiological events leading to the disruption of myelin sheath in MS. However, there are emerging evidences supporting gray matter involvement and degeneration in MS. The investigation of T cell function in the pathogenesis of deep gray matter damage is necessary. Here, we employed RSA59 (isogenic recombinant strain of MHV-A59) induced experimental neuroinflammation model to compare the disease in CD4^{-/-} mice with CD4^{+/+} mice at days 5, 10, 15, and 30 p.i. Viral titer estimation, nucleocapsid gene amplification and viral anti-nucleocapsid staining confirm enhanced replication of the virions in the absence of functional CD4⁺ T cells in the brain. Histopathological analyses showed an elevated susceptibility of CD4^{-/-} mice to axonal degeneration in the CNS with augmented progression of acute poliomyelitis, and dorsal root ganglionic inflammation rarely observed in CD4^{+/+} mice. Depletion of CD4⁺ T cells shows unique pathological bulbar vacuolation in the brain parenchyma of infected mice with persistent CD11b⁺ microglia/macrophages in the inflamed regions on day 30 p.i. In summary,

the current study suggests that CD4⁺ T cells are critical for controlling acute stage poliomyelitis (gray matter inflammation) and chronic axonal degeneration, inflammatory demyelination due to loss of protective anti-viral host immunity.

#: Equal contribution

Debanjana Chakravarty and Fareeha Saadi contributed equally to this work. Author order was determined based on the relatedness of the work with Debanjana Chakravarty's PhD thesis.

*** Corresponding authors:**

Kenneth S. Shindler: Departments of Ophthalmology and Neurology, University of Pennsylvania, Scheie Eye Institute, Philadelphia, PA 19104, USA. E-mail: Kenneth.Shindler@uphs.upenn.edu

Jayasri Das Sarma: Department of Biological Sciences, Indian Institute of Science Education and Research Kolkata, Mohanpur-741246, India. E-mail: dassarmaj@iiserkol.ac.in

KEYWORDS: CD4⁺T cells, Microglia, MHV infection, mCoV, Neuroinflammation, Innate immune response, Demyelination, Host Immunity

IMPORTANCE

The current trend in CNS disease biology is to understand the neural cell-immune interaction to investigate the underlying mechanism of neuroinflammation, rather than focusing on peripheral immune activation. Most studies in MS are targeted toward understanding the involvement of CNS white matter. However, the importance of gray matter damage has become critical in understanding the long-term progressive neurological disorder. Our study highlights the importance of CD4⁺T cells in safeguarding the neurons against axonal blebbing and poliomyelitis from murine Betacoronavirus-induced neuroinflammation. Current knowledge of the mechanisms that lead to gray matter damage in MS is limited, because the most widely used animal model EAE does not present this aspect of the disease. Our results thus, add to the existing limited knowledge in the field. We also show that the microglia, though important for the initiation of neuroinflammation, cannot establish a protective host immune response without the help of CD4⁺ T cells.

INTRODUCTION

Neuroinflammation is the cardinal signature of several complex and multi-faceted central nervous system (CNS) disorders. CNS inflammation is known to be initiated mainly by the brain's resident innate immune cells, the microglia, which rapidly respond to an infectious agent or any perturbation in the CNS. Via the secretion of chemokines and cytokines, they direct the extravasation of several myeloid cells, including neutrophils, monocytes/macrophages, and dendritic cells, which in turn promote the entry and activation of adaptive immune responsive T cell populations into the CNS(1-4).

Regulation of T cells is central to understanding the cellular and humoral immunity in neuroinflammation. So far, most studies have demonstrated the destructive pathogenic effects of encephalitogenic T cells in neurodegeneration. For example, Multiple sclerosis (MS the most common neurological disease of young adults is characterized predominantly by self-reactive myelinolytic T cell-mediated autoimmune destruction of the myelin sheath (5-10). Likewise, in an experimental animal model of MS, Experimental autoimmune encephalomyelitis (EAE), the disease mainly depends on the infiltration of pathogenic CD4⁺ T cells, which are primarily of Th1 and Th17 types (11-19). Studies have also shown a pathogenic role of myelin-specific CD8⁺ T cells in the inflammatory lesions in EAE mice brains (20-22). A Mouse hepatitis virus (MHV) (V5A13.1) model of induced neuroinflammation showed a significant reduction in the severity of inflammation and demyelination in CD4^{-/-} mice at days 12-21 p.i. compared to both CD8^{-/-} and wild type mice (23). Adoptive transfer of CD4⁺T cells and CD8⁺T enriched splenocytes differentially affect the state of inflammation and demyelination in MHV-JHM infected RAG^{-/-} mice and induction of donor splenocytes with a depleted population of both CD4 and CD8⁺ T cells in JHM infected RAG^{-/-} mice prevents demyelination (24). However, recent advances have shown that the prevalence of activated adaptive immune responses are not restricted to neuroinflammatory myelin degeneration as seen in MS but translates across classic neurodegenerative disorders such as Alzheimer's disease (AD), Parkinson's disease (PD) and Amyotrophic lateral sclerosis (ALS) (25, 26) (27, 28) (29) (30).

With the shift in the paradigm of CNS immunology and the discovery of CNS meningeal lymphatic vessels, several studies also suggested that CD4⁺ T cells may provide protective immunity against cognitive and motor disabilities in neurodegenerative disorders (31) (32). Activated CD4⁺ T cells also help in limiting MHV-JHM replication within the CNS (33). Either CD4 or CD8 deletion in Theiler's Murine Encephalomyelitis (TMEV) resistant B6 strain

92 makes the mice susceptible to disease and shows increased viral persistence and demyelination
93 (34). The current research trend is thus targeted toward understanding the differential
94 mechanisms that regulate the balance between neuroprotection and neurodestruction conferred
95 by CD4⁺ T cells.

96 Several studies have demonstrated the accumulation of microglia/macrophages in the vicinity
97 of reactive CD4⁺ T cells in CNS lesions during neurodegeneration (4, 30, 35-37). While ample
98 literature supports CD4⁺ T cells interaction with CNS resident microglia and/or infiltrating
99 myeloid-specific monocytes/macrophages as the primary mechanisms underlying white matter
100 damage in the early relapsing-remitting stage of MS, one cannot overlook their function behind
101 immune mediated gray matter atrophy.

102 The current study is focused on understanding the potential protective role of CD4⁺ T cells on
103 microglial activation and their cooperative effect on both white and gray matter damage
104 following infection with a neurotropic isogenic spike protein recombinant strain of
105 Betacoronavirus MHV, RSA59. Intracranial infection of C57BL/6 mice with RSA59 results in
106 a biphasic disease, characterized by acute hepatitis and meningoencephalomyelitis followed by
107 chronic immune-mediated demyelination and concomitant axonal loss, which mimics specific
108 pathologies of the human demyelinating disease MS (38-40). RSA59 induced acute
109 neuroinflammation comprises mixed populations of astrocytes and inflammatory cells, mainly
110 microglia/macrophages and a smaller population of T lymphocytes (40-44). As early as day 3
111 post-infection (p.i.), peripheral leukocytes start to infiltrate the CNS, beginning with the cells
112 of the innate immune response predominantly myeloid cells such as neutrophils and
113 monocytes/macrophages. Lymphoid cells, including CD4, CD8, and NK T cells start to appear
114 in the CNS at day 5 p.i. and their infiltration peaks at day 7 p.i. followed by the start of viral
115 clearance (Fig. 1). While CD8⁺ T cells begin to disappear as early as day 10 p.i. and NK T cells
116 reduce in number, a significant number of CD4⁺ T cells are present in the inflamed brain even
117 at day 16 p.i. (Fig. 1). While inflammation resolves and infectious virus particles clear from
118 the brain, Iba1⁺ macrophages/microglia persist significantly within the demyelinating plaques
119 in the spinal cord white matter and are known to cause direct myelin stripping (40). Recent
120 Affymetrix microarray analysis in the spinal cord of RSA59 infected mice showed elevated
121 expression of inflammatory mediators during the acute stage of infection. Interestingly,
122 conventional T and B cell markers showed no or insignificant upregulation (45, 46). Expression
123 of adaptive immune responsive genes showed prominent upregulation during the chronic phase

(46). The most striking associations were observed between CD3, CD45, and MHCII expression, which promote the communication between innate and adaptive immune systems via microglia-CD4⁺T cell signalling.

Current study employs a CD4 knock out strain in the background of C57BL/6 mice (CD4^{-/-}). In comparison to the wild type C57BL/6 mice (CD4^{+/+}), infection of CD4^{-/-} mice produces an exaggerated disease course in association with enhanced viral replication and prolonged viral persistence. Moreover, CD4^{-/-} mice are more susceptible to chronic inflammation, and axonal degeneration compared to CD4^{+/+} mice, and CD11b⁺ macrophages/microglia show persistent activation even during the chronic disease phase. Our results suggest a novel neuroprotective role of CD4⁺ T cells in the MHV induced demyelinating model of MS unlike the EAE model where T cells have a predominantly pathogenic role.

RESULTS

Mice were inoculated with isogenic EGFP expressing RSA59 as described in the materials and methods section. Experimental mice were monitored daily for the development of clinical signs and symptoms. The majority of CD4^{+/+} mice displayed low disease scores ranging from 0.5 to 1, indicated by ruffled fur and occasionally present the hunch back phenotype as observed previously (47). 100 % mice survived until day 30 p.i as observed . Though not significantly different, CD4^{-/-} mice showed a slightly higher disease score of 1.5 to 2 indicated by hind limb weakness in addition to hunch back, the symptoms started appearing as early as day 3-5 p.i., however, almost 90% mice survived until day 30 p.i. The scoring system has been discussed in the materials and methods section.

The absence of functional CD4⁺ T cells does not alter acute stage hepatitis and meningoencephalomyelitis but shows gray matter involvement in the form of poliomyelitis and Dorsal Root Ganglion inflammation.

The current study initially investigated differences in phenotypic or pathological symptoms as well as basal level of inflammation at the tissue level between mock infected CD4^{+/+} and CD4^{-/-} mice. No significant differences were observed at the phenotypic level. Conventional light microscopy data analysis at H& E staining sections from liver, brain and spinal cord revealed that mock infected (MI) CD4^{+/+} and CD4^{-/-} mice presented only a basal level of inflammation (if any) in all the three tissue types (Fig 2). Mock infected CD4^{-/-} mice did not show any

differential phenotypic or histopathological features concerned for this study. All experiments were conducted using age matched CD4^{+/+} and CD4^{-/-} mice.

To examine the degree of inflammation in CNS and non-CNS tissues, MI and infected CD4^{+/+} and CD4^{-/-} mice were sacrificed at two-time points, day 5-6 p.i. (onset of the peak of neuroinflammation) and day 30 p.i. (chronic phase of inflammation). The liver, brain, and spinal cord tissues were harvested and fixed in 4 % paraformaldehyde and paraffin embedded.

During the acute phase of infection, comparable, multiple foci of moderate to severe necrotizing, and non-necrotizing hepatitis were observed in both CD4^{+/+} and CD4^{-/-} mice (Fig. 3a). During the chronic phase, hepatitis nearly resolved, but the number of remnant hepatic lesions were more in CD4^{-/-} mice (Fig. 3b). The Hepatic Activity Index showed no significant difference at day 6 and 30 p.i. between CD4^{+/+} and CD4^{-/-} mice (Fig. 3b).

H&E stained brain sections from RSA59 infected CD4^{+/+} and CD4^{-/-} (Fig. 4a) mice demonstrated focal acute encephalitis, meningitis, intra-parenchymal perivascular lymphocytic cuffing, and microglial nodule formation at the acute phase of infection. Corresponding serial brain sections immunohistochemically stained with anti-CD45 (leukocyte common antigen, LCA) confirmed similar levels of inflammatory cells in the brain parenchyma of CD4^{+/+} (2.691 ± 0.4561) and CD4^{-/-} (2.485 ± 0.3849) mice(48). H&E staining of both CD4^{+/+} and CD4^{-/-} (Fig. 4b) infected spinal cords showed myelitis. Quantification of the staining intensity suggests that corresponding regions were equally immunoreactive for CD45, indicating the comparable infiltration of mononuclear cells in CD4^{+/+} (1.176 ± 0.1958) and CD4^{-/-} mice (1.355 ± 0.1947). However, the consequent anti-CD11b (pan-macrophage marker) immunohistochemistry revealed significantly fewer macrophage/microglia in the brains and spinal cords of CD4^{-/-} mice (0.6067 ± 0.1260 , **** $p < 0.0001$ and 0.258 ± 0.07078 , ** $p < 0.01$ respectively), as compared to CD4^{+/+} mice (4.749 ± 0.3981 , and 1.110 ± 0.3007 , respectively) (Fig. 5). Moreover, apart from the white matter myelitis in both infected CD4^{+/+} and CD4^{-/-} mice, CD4^{-/-} mice showed evidence of acute poliomyelitis (gray matter inflammation) and dorsal root ganglionic inflammation which were rarely observed in CD4^{+/+} mice at the acute phase of infection (Fig. 6). Average inflammation scores, based on H&E, are shown in Table I and II.

The absence of CD4⁺ T cells impairs RSA59 clearance from the brain tissue.

To assess the role of CD4⁺ T cells in virus clearance, viral titer, viral nucleocapsid gene amplification, in situ viral antigen distribution and mRNA level of anti-viral pro-inflammatory cytokines /chemokines were evaluated.

RSA59 titer kinetics was compared in the brains of CD4^{-/-} and CD4^{+/+} mice, and the values were expressed as log₁₀ PFU/ gram of tissue. In both mouse strains, the virus replicated efficiently in the brain at day 5 p.i. (10^{5.8} PFU/gm in CD4^{-/-} versus 10^{6.1} PFU/gm in CD4^{+/+}). By day 10 p.i. CD4^{-/-} mice averaged almost 1-log-higher viral titre (10⁵ PFU/gm versus 10^{3.9} PFU/gm, *p= 0.016) than CD4^{+/+} mice. On day 15 p.i. there were no detectable viral PFUs in CD4^{+/+} mice, however, a significant number of infectious viral PFUs were observed in CD4^{-/-} mice (10^{4.6} PFU/gm, ****p=0.0001) (Fig. 7a).

To further confirm whether differences in viral replication might affect viral infection, qRT-PCR of viral N-gene (nucleocapsid) from brain tissues from MI, CD4^{+/+}, and CD4^{-/-} infected mice was performed. As shown in Fig. 7b, viral persistence is comparable in both CD4^{+/+} and CD4^{-/-} mice (1.02 fold ± 0.176) at day 5 p.i. At day 10 and day 15 p.i., the N-gene transcript shows significant upregulation (10.230 folds ± 2.677, **p= 0.003 and 23.247 folds ± 5.204, ****p< 0.0001, respectively), in CD4^{-/-} mice compared to CD4^{+/+}.

To determine the spread of infectious viral particles in situ, immunohistochemical analysis of viral anti-nucleocapsid antigen was performed on sections of infected brains obtained from CD4^{+/+}, CD4^{-/-}, and MI mice at the acute and chronic phases of infection. In MI mice, viral antigen was neither observed at day 6 nor at day 30 p.i. as expected (Fig. 7c). Post-intra-cranial inoculation, RSA59 replicates profusely in CD4^{+/+} mice and spreads rapidly from the lateral geniculate nuclei to several regions of the brain, including the olfactory bulb, basal forebrain, cerebral cortex, anterior commissure, brain stem and deep cerebellar white matter. By day 6 p.i., viral antigen becomes restricted to the midbrain, pons, and deep cerebellar white matter in the current study (data not shown). Similar viral anti-nucleocapsid antigen staining was observed in infected CD4^{-/-} mice at day 6 p.i. Day 30 post infected brains of CD4^{+/+} mice showed significantly reduced viral antigen staining as expected, whereas a considerable number of cells remained positive for viral anti-nucleocapsid antigen in the CD4^{-/-} mice (Fig. 7c).

Moreover, Interferon gamma (IFN-γ) mRNA expression was significantly higher at day 5 p.i. in CD4^{-/-} mice (2.45 folds ± 0.59, **p=0.0020), Fig. 7d, in comparison to CD4^{+/+} mice,

indicating higher viral replication in CD4^{-/-} mice. Similarly, peripheral leukocyte chemoattractant IFN- γ inducible CXCL10 (a C-X-C chemokine) mRNA expression remained significantly upregulated even at day 10 p.i. (5.102 folds \pm 1.253, ***p=0.0008) and day 15 p.i. (2.965 folds \pm 0.858, *p=0.015) in the infected CD4^{-/-} mice (Fig. 7e) as compared to CD4^{+/+} mice. Also, anti-viral Tumour Necrosis Factor alpha (TNF- α) mRNA expression was observed to be significantly upregulated at all time points in CD4^{-/-} mice, in comparison to CD4^{+/+} mice (6.372 folds \pm 1.10, ****p<0.0001 at day5, 37.949 folds \pm 9.534, ****p=0.00018 at day 10, and 7.348 folds \pm 1.675, ****p<0.0001 at day 15), Fig. 7f. At the same time, CD4^{-/-} mice displayed lower levels of RANTES (Regulated upon Activation, Normal T Cell Expressed and Presumably Secreted) or CCL5 (a C-C chemokine, involved in trafficking of macrophage/monocytes into the CNS) mRNA transcripts at day 5 p.i. (0.523 folds \pm 0.124, **p<0.01 and day 10 p.i. (0.544 folds \pm 0.214, *p<0.05) in comparison to CD4^{+/+} mice (Fig. 7g)

Viral plaque assays and qRT-PCR of viral N-gene and antiviral-cytokines and chemokines expression (IFN- γ , TNF- α , CXCL10) at day 5, 10 and 15 p.i in corroboration with the viral anti-nucleocapsid antigen staining at day 30 p.i. confirmed prolonged persistence of RSA59 in the absence of functional CD4 in brain tissue.

The absence of CD4⁺ T cells exacerbates CNS inflammation and myelin loss at the chronic stage of inflammation.

The role of functional CD4⁺ T cells in demyelination was next examined by histopathological analysis of day 30 post-infected spinal cords from CD4^{+/+} and CD4^{-/-} mice. In CD4^{+/+} mice, inflammation was observed in the dorsal/posterior columns, anterior horn and/or the lateral descending tracts. H&E staining highlights the inflammation in the ventrolateral white matter. In contrast, CD4^{-/-} mice demonstrated vacuolar pathology with swollen axons throughout the white matter, involving the ventral and lateral descending tracts upon H& E staining (Fig. 8a). Corresponding inflamed regions from serial sections also showed myelin loss by LFB staining in both CD4^{+/+} and CD4^{-/-} mice. The degree of demyelination was significantly higher in the CD4^{-/-} mice (20.45 \pm 2.174, ****p<0.0001) compared to CD4^{+/+} mice (6.008 \pm 1.375) (48) (Fig. 8b). CD45 immunoreactive inflammatory cells were present within the demyelinating plaques in both CD4^{+/+} and CD4^{-/-}, however the extent of inflammation was considerably greater in CD4^{-/-} (2.812 \pm 0.1122, ****p<0.0001) mice in comparison to the CD4^{+/+} mice (0.5509 \pm 0.08550) (Fig. 8c). Interestingly, in contrast to the acute phase of infection, CD4^{-/-}

mice (1.237 ± 0.1646 , *** $p < 0.001$) spinal cord showed highly significant CD11b microglia/macrophage expression, in comparison to CD4^{+/+} mice (0.4175 ± 0.09144). (Fig. 8d)

Quite strikingly, in contrast to the brains of CD4^{+/+} (Fig. 9a) mice, CD4^{-/-} mice exhibited extensive vacuolation in the brain stem and the deep cerebellar white matter tracts which has not been observed in previous studies. No significant differences were observed in CD45 staining between the two groups (Fig. 9b). Large numbers of CD11b positive microglia/macrophages were observed in the vicinity of the vacuolated regions in CD4^{-/-} mice (5.251 ± 0.5298 , **** $p < 0.0001$) as compared to CD4^{+/+} mice (2.220 ± 0.1639) (Fig. 9c).

The Absence of CD4⁺ T cells aggravates axonopathy

One-micron thick sections of glutaraldehyde fixed brains and spinal cords from RSA59 infected CD4^{-/-}, CD4^{+/+}, and MI CD4^{-/-} mice were stained with toluidine blue. MI CD4^{-/-} did not show any visible signs of inflammation (Fig. 10) or spinal cord damage. Infected CD4^{-/-} mice exhibited vacuolation and axonal degeneration in the posterior columns (Fig. 11a, b). Electron microscopy of the vacuolated brainstem lesions in CD4^{-/-} mice revealed that the vacuolation represents numerous swollen degenerating axons, and few inflammatory cells (lymphocytes and macrophages). There was no evidence of isolated demyelination (myelin loss with relative axonal preservation) (data not shown). Similarly, electron micrographs of the spinal cord white matter lesions (Fig. 11c, d) also showed axonal degeneration and a lack of demyelination. No inflammatory cells (lymphocytes and macrophages) were present within the areas of white matter damage (Fig. 11c).

In the absence of CD4⁺ T cells, mice show differential expression of inflammatory cytokines.

The inflammatory cells in the demyelinating lesions induced by RSA59, exhibit variable expression of pro- and anti-inflammatory cytokines. Expression of pro-inflammatory IL-6, IL-12p40, and anti-inflammatory IL-10 were examined in RSA59 infected mouse brains. Quantitative PCR results revealed that IL-6 expression was significantly higher in CD4^{-/-} compared to CD4^{+/+} mice both at day 5 (6.742 folds ± 1.955 , **** $p < 0.0001$) and day 10 p.i. (4.24 folds ± 0.912 , **** $p < 0.0001$), and subsequently declines at day 15 p.i. in both groups of mice (Fig. 12a). IL-10 expression patterns, as revealed by real-time PCR, showed similar expression in the RSA59 infected CD4^{+/+} and CD4^{-/-} mice at day 5 p.i. However, at days 10 (2.579 folds ± 0.72 , ** $p = 0.003$) and 15 p.i. (2.58 folds ± 0.363 , **** $p < 0.0001$) CD4^{+/+} mice

showed significantly elevated expression of IL-10 compared to infected CD4^{-/-} mice (Fig. 12b). IL-12p40 mRNA expression demonstrated no considerable differences between CD4^{+/+} and CD4^{-/-} mice following RSA59 infection (data not shown). Together the expression patterns of IL-6 and IL-10 indicate a robust inflammatory environment in the brains of CD4^{-/-} mice.

The absence of CD4⁺ T cells influences macrophage polarization.

Using the classical M1/M2 nomenclature of macrophage polarization, it was observed that mRNA expression of classical M1 macrophage (pro-inflammatory) markers such as CD86 and Bruton's tyrosine kinase (Btk) were significantly reduced in infected CD4^{-/-} mice in comparison to CD4^{+/+} mice at day 5 p.i (0.445 folds \pm 0.128, ***p<0.001 and 0.545 folds \pm 0.134, **p<0.01, for CD86 and Btk respectively) (Fig. 12c,d). But, as the course of disease progressed toward the chronic phase, microglia/macrophages in the infected CD4^{-/-} mice showed an M2 phenotype (anti-inflammatory) in contrast to the CD4^{+/+} mice, as observed by the significant upregulation in the mRNA expression of M2 macrophage marker CD163 at day 15 p.i. (2.018 folds \pm 0.392, ****p<0.0001) (Fig. 12e).

DISCUSSION

The CNS is no longer considered an immune-privileged site (49). A significant number of peripheral CD4⁺ T cells patrol the cerebrospinal fluid (CSF) in order to detect the presence of potential harmful pathogens (50-52). If these T cells do not encounter their cognate antigen, they take the lymphatic route to exit the CNS. However, they will infiltrate the CNS parenchyma upon sensing any sign of neuroinflammation (52, 53). MHV infection in mice is an established archetype animal model used to understand the demyelination pathology in MS. In this study, we present a protective role of CD4⁺ T cells in the viral induced neuroinflammatory demyelination, in contrast to the pathogenic role of CD4⁺ T cells in MS (54) and its autoimmune experimental model EAE. Activated myelinolytic CD4⁺ T cells have been observed in the blood and cerebrospinal fluid (CSF) of MS patients (7); Additionally, MS lesions have been widely associated with the presence of both CD4⁺ and CD8⁺ T cells (55). These autoreactive T cells induce a Th-1 response, majorly targeted against PLP, and can worsen the disease progression in the patients (56-58). Considering their well-accepted pathogenic role in MS, classical immuno therapies are devised to silence the CD4⁺ T cell mediated attack on the myelin to repair the damage caused to the myelin sheath. Our study

highlights a quite opposite, protective role of CD4⁺T cells in a virus induced etiology of demyelination in MS.

In this study, we present evidences to show that spatio-temporal infiltration of CD4⁺ T cells in the CNS and their dynamic equilibrium with brain resident microglia may influence the progression, severity, and amelioration of white and gray matter inflammation in a neurotropic virus model. The most widely used experimental model of MS, EAE, holds good only for understanding the mechanisms of white matter injury and does not recapitulate the aspects of gray matter damage.

The RSA59-induced demyelinating model is unique, it involves both white and gray matter inflammation. The onset of the disease is initiated via orchestration of innate immune genes in the acute phase to clear the virus and restore homeostasis and then gradually progress via adaptive immunity during the chronic phase (45). RSA59 induced demyelination is dissimilar to other conventional demyelinating models that are explicitly driven by adaptive immune responses, with its array of specialized T cells (CD4⁺ and CD8⁺) and myelin antigen-specific antibodies (20, 59, 60). Dynamic host immune responses involving CD4⁺ helper T cells are needed for recovery from infections. While CD4⁺ T cells are helpers for the development of a complete adaptive immune response, they are also required for enhancing innate immune effector functions. To assess the role of CD4⁺ T cells in the innate and adaptive immune responses and their interactions with microglia/macrophages following RSA59 infection, the current study compared CD4^{-/-} mice and wild-type mice. The results showed a critical role of CD4⁺ T cells in the pathogenesis of RSA59 induced neuroinflammation. We observed the following: i) Absence of CD4⁺ T cells caused no change in acute encephalitis; but CD4^{-/-} mice showed a significant reduction in CD11b positive microglia/macrophages; ii) viral replication was higher and viral transcripts were persistent in CD4^{-/-} mice, even at day 30 p.i.; iii) CD4^{-/-} mice showed an augmented susceptibility toward chronic phase encephalitis and demyelination. Furthermore, CD4^{-/-} mice, presented with poliomyelitis, bulbar (brainstem) vacuolation of the neuropil, and dorsal root ganglionic inflammation, a finding rarely observed in CD4^{+/+} mice; iv) a strikingly higher number of CD11b positive microglia/macrophages were present in the CD4^{-/-} mice at the chronic infection phase. These microglia/macrophages were disseminated throughout the inflamed regions of white matter and in the areas of gray matter, both in the brain and spinal cord at the chronic infection phase; and v) Electron microscopy revealed axonal degeneration in the spinal cords of CD4^{-/-} mice even in the absence of

inflammation, suggesting that white matter degeneration occurs secondary to neuronal injury without a direct attack of inflammatory cells upon spinal cord myelin sheaths.

Our results also revealed substantially higher mRNA expression levels of IFN γ , TNF α , and IFN inducible leukocyte chemoattractant CXCL10 in the CD4^{-/-} mice in comparison to CD4^{+/+} mice which is likely a response to recruit further peripheral lymphocytes into the CNS to combat the persistent viral load in the former. The increased and uncontrolled viral replication contributes to severe inflammation and neuronal cell body damage observed in the gray matter of the spinal cord and dorsal root ganglion of the CD4^{-/-} mice. Elevated mRNA levels of pro-inflammatory cytokine IL-6 at day 5 and 10 p.i. along with persistent viral load signifies a robust pro-inflammatory environment in the CNS of CD4^{-/-} mice. Expression of the anti-inflammatory cytokine IL-10 remains almost constant throughout the study in CD4^{+/+} mice, while its expression in CD4^{-/-} is consistently low, suggesting that CD4⁺ T cells serve as one of the key sources of IL-10 production.

Apart from this, it was interesting to note that anti-viral chemokine CCL5 or RANTES (macrophage/monocyte chemoattractant) was downregulated in CD4^{-/-} mice at day 5 and 10 p.i., perhaps as a result of which a significant reduction in CD11b positive inflammatory cells was observed in the brains and spinal cords at the acute phase of inflammation. Nevertheless, overall encephalitis at the acute phase, as shown by CD45 staining, was comparable in both CD4^{+/+} and CD4^{-/-} mice, suggesting that the initial inflammation in the CNS is independent of CD4⁺ T cells. This finding also hints that the fewer numbers of CD11b⁺ cells might be the result of dampened infiltration of monocyte/macrophages in the absence of functional CD4⁺ T cells and the CD11b⁺ cells observed in the CNS might correspond to the brain resident microglia.

The function and role of microglia as mediators of homeostasis in the CNS is well established (61). They not only act as custodians of CNS immunity but also protect neurons during development and monitor synaptogenesis (62). However, during pathological conditions, microglia attain a signature pro-inflammatory state that is directed toward the clearance of toxic substances from the CNS (63, 64). M1 or classically activated microglia can also induce the activation of A1 astrocytes, which develop altered ability to promote neuroprotection (65). A2 astrocytes are activated by M2 microglia (alternatively activated) and help in CNS repair and protection (66). Examination of mRNA expression revealed a higher expression of pro-inflammatory M1 markers CD86 and Btk in the CNS of CD4^{+/+} mice during the acute infection.

371 CD163 mRNA transcripts increased in expression in the CD4^{+/+} mice during day 10 p.i. and
372 then declined with the restoration of homeostasis, but CD4^{-/-} mice showed a significant increase
373 in the expression of CD163 mRNA even at day 15 p.i. suggesting that the CD11b⁺
374 microglia/macrophages present during the transition phase (from acute to chronic) in the CNS
375 might be of the M2 phenotype (anti-inflammatory) attempting to combat the prolonged viral
376 persistence and restore homeostasis to prevent further tissue damage, but fail to do so without
377 the help of CD4⁺T cells. Though M2 microglia/macrophages are categorized as anti-
378 inflammatory, they are also reported to have high phagocytic ability. Their activation and
379 persistence might, therefore, promote direct myelin stripping as previously reported (40)
380 leading to significantly greater demyelination and axonal loss in the CD4^{-/-} mice.

381 An interesting question that remains to be answered is if the infiltration of
382 monocyte/macrophages is impeded in the first place, why is there a higher expression of CD11b
383 positive cells in the CNS of CD4^{-/-} mice during the chronic phase? To answer this, future
384 experiments are aimed at performing immunophenotyping of the inflammatory cells, using
385 flow cytometry in the CD4^{-/-} mice, to explicitly decipher whether the cells present at the chronic
386 phase are predominately peripherally recruited monocytes/macrophages or the activated
387 resident phagocytic microglial cells of the CNS. So far, flow cytometric analysis in CD4^{+/+}
388 mice has shown the presence of a significant population of CD11b^{hi}/ CD45^{lo} (microglia) at
389 day 30 p.i. but very little or no CD11b expressing CD45 high monocyte/macrophages in the
390 CNS (data not shown). We, therefore, expect the CD11b⁺ cells found in the CNS at day 30 in
391 the CD4^{-/-} mice to be microglia and not peripherally recruited myeloid cells.

392 For this study, we have opted for a mouse strain (B6.129S2-Cd4^{tm1Mak}/J) where the
393 functionality of CD4⁺ T helper cells was disrupted. The development of CD8⁺ T cell and
394 myeloid components was unaffected. 90% of the circulating T cells were CD8⁺ and their
395 cytotoxic activity was within normal ranges (67). Despite the presence of functional CD8⁺ T
396 cells, viral clearance was substantially delayed. Thus, our studies suggest a vast preponderance
397 of CD4⁺ T cells over CD8⁺ T cells in maintaining the homeostasis upon RSA59 induced
398 neuroinflammation.

399 In conclusion, our results demonstrate that CD4⁺ T cells are necessary for eliminating viral
400 particles, promoting microglial polarization toward anti-inflammation, and controlling chronic
401 progressive axonal degeneration. The current study also highlights the importance of CD4⁺T
402 cells beyond the classic inflammatory lesions of the white matter tract. We have shown that

gray matter inflammation in the form of poliomyelitis is significantly exacerbated in the absence of CD4⁺ T cells. Moreover, we show that the imprinting of the microglia/macrophage-mediated inflammatory innate immune response on the consequent protective adaptive immunity requires functional CD4⁺ T cells. This communication between microglia and T cells is a highly regulated, interdependent, and bidirectional process and is critical for the establishment of an effective immune response. Although innate anti-viral immune responses by microglia are crucial in controlling the initial CNS viral dissemination, virus-specific T cells are essential to eliminate the virus and provide indispensable neuroprotection. Further studies will be conducted to understand the nexus between CNS resident microglia/monocyte-derived macrophages with infiltrating activated T helper cells at the molecular level through immune-coregulatory CD40-CD40 ligand (L) pathway. This dyad is broadly recognized for its essential role in immune regulation and homeostasis. Our studies will be focused to examine such interactions at the molecular level using CD40 and CD40L deficient mice in the outcome of inflammatory demyelination. Most MS therapies are aimed at preventing damage to myelin by regulating the multiple components of adaptive immune system, especially the T cell subsets (Th1, Th2, Th17, CD8⁺, NKT, CD4⁺CD25⁺ T regulatory cells) and B cells. Current therapies have only been able to reduce the number and rate of MS lesion formation and are only partially efficacious(68). Understanding the role of T cells in a viral induced model of MS is thus critical to design more robust therapeutics. Together these studies can help to expand our knowledge intended to use CD4 mediated immune therapy as a potential treatment of MS, depending on its etiology and the initiation of the pathology.

MATERIALS AND METHODS

Virus, Inoculation of mice and Experimental design

Recombinant isogenic demyelinating (DM) strain of MHV-A59, RSA59, was used to infect mice as formerly described (39). Four to five-week old, MHV-free, CD4^{+/+/+} C57BL/6 (B6) mice (Jackson Laboratory) and CD4^{-/-} (B6.129S2-Cd4^{tm1Mak}/J) mice (Jackson Laboratory, Stock no. 002663) were used for the study. The CD4^{-/-} mice obtained from Jackson's laboratory is homozygous for the Cd4^{tm1Mak} targeted mutation, have a significant blockade in the CD4⁺ T-cell development and show an MHC class II restricted T helper cell activity(67). The mice were inoculated intracranially with 25,000 (50% of LD50) PFU of RSA59 strain as described previously. Likewise, mock-infected controls for CD4^{+/+} and CD4^{-/-} mice were inoculated with an uninfected cell lysate (PBS+0.075% BSA) at an equivalent dilution. Mice were

monitored daily post infection (p.i.) for disease signs and symptoms. Clinical disease severity was graded using the following scale: 0, no disease symptoms; 1, ruffled fur; 1.5, hunched back with mild ataxia; 2, Ataxia, balance problem and hind limb weakness; 2.5 one leg completely paralyzed, motility issue but still able to move around with difficulties; 3, severe hunching/wasting/both hind limb paralysis and mobility is severely compromised; 3.5 Severe distress, complete paralysis and moribund 4, dead (47).

For EM, histopathological, and immunohistochemical analyses mice were sacrificed at the acute infection phase, i.e. on day 5-6 (four mice per group), and chronic infection phase, i.e. day 30 (five mice per group) post-infection. For RNA and protein studies and viral titer estimation, animals were sacrificed (3 mice per group) on days 5, 10 and 15 post-infection.

Estimation of Viral Replication

Mice were euthanized on days 5, 10 and 15 post-infection and perfused transcardially with 20 ml of sterile PBS. Brains were harvested for determination of viral titers and placed into 1 ml of isotonic saline containing 0.167% gelatin (gel saline). Brain tissues were weighed and kept frozen at -80°C until titred. Tissues were subsequently homogenized, and viral titers were quantified by standard plaque assay protocol on tight monolayers of L2 cells as described previously with minor modifications (39).

Histopathology and Immunohistochemical Analysis

Mice were sacrificed at day 6 and day 30 post-infection. Following transcardial perfusion with PBS and 4% paraformaldehyde, liver, brain, and spinal cord tissues were harvested and embedded in paraffin. Five-micron thick sections of the embedded tissues were prepared and stained with Hematoxylin and Eosin for histopathologic analysis. Luxol fast blue (LFB) staining was performed to evaluate demyelination in the brain and spinal cord tissues, as described previously with minor modifications (40).

Immunohistochemical staining of brain and spinal cord tissue sections used the following primary antibodies - 1:10000 dilution of anti-CD11b (Abcam, Cat #:ab133357), 1:200 dilution of anti-CD45 (LCA; leukocyte common antigen, BD Pharmingen Cat#:550539) and 1:40 dilution of monoclonal antibody directed against the nucleocapsid protein (N) of MHV (monoclonal antibody clone 1-16-1 provided by Julian Leibowitz, Texas A&M University). Bound primary antibodies were detected by an avidin-biotin immunoperoxidase technique

(Vector Laboratories) using 3, 3-diaminobenzidine as the substrate. Control slides from mock-infected mice were stained in parallel. All slides were coded and read in a blinded manner by the same investigator, as described previously with minor modifications (40).

H&E Sections were assessed for inflammation in the following manner: 0, none; 1, few inflammatory cells; 2, organization of perivascular infiltrates; and 3, increasing severity of perivascular cuffing and formation of microglial nodules, and represented in Table 1 (47).

Quantification of histopathological sections

The number of hepatic lesions were counted per section and averaged for each mouse at each time point (both acute and chronic phase of inflammation). The functional scoring of the inflammatory lesions in the liver was characterized as the Hepatic activity index (HAI). Degree of activity was categorized as portal inflammation; Interphase hepatitis (Piecemeal necrosis); Focal (Spotty) necrosis, apoptosis, and focal inflammation; and Confluent necrosis. Scores from 0-6 were allotted for each category based on the modified Knodell's HAI, commonly referred to as the Ishak system (69).

Image analysis was performed using the basic densitometric thresholding application of Fiji (Image J, NIH Image, Scion Image) as described previously (48). Briefly, image analysis for CD45 and CD11b stained sections was performed by capturing the images at the highest magnification (4X-for brain, 10X-for spinal cord) such that the entire section (i.e., scan area) can be visualized within a single frame. The RGB image was deconvoluted into three different colours to separate and subtract the DAB-specific staining from the background H&E staining. The perimeter of each brain and spinal cord tissue was digitally outlined, and the area was calculated in μm^2 . A threshold value was fixed for each image to make sure that all antibody marked cells are taken into consideration. The amount of CD45, and CD11b staining was termed as the '% area of staining'.

To determine the area of demyelination, LFB-stained spinal cord cross-sections from each mouse were chosen and analyzed using Fiji software (Image J 1.52g). The total perimeter of the white matter regions in each cross-section was marked and calculated by adding together the dorsal, ventral and anterior white matter areas in each section. Also, the total area of the demyelinated regions was outlined and collated for each section separately. The percentage of spinal cord demyelination per section per mouse was calculated.

Gene Expression: RNA Isolation, Reverse transcription and quantitative Polymerase chain reaction

RNA was extracted from brain tissues (flash-frozen) of RSA59 infected CD4^{+/+} and CD4^{-/-} and mock-infected mice (3 from each group at days 5, 10 and 15 p.i.) using the Trizol isolation protocol following transcardial perfusion with DEPC treated PBS. The total RNA concentration was measured using a NanoDrop ND-100 spectrophotometer. 1µg of RNA was used to prepare cDNA using a High Capacity cDNA Reverse Transcription Kit (Applied Biosystems). Quantitative Real-time PCR analysis was performed using DyNAmo Color Flash SYBR Green qPCR kit (Thermo Scientific) in a Step One plus Real-time PCR system (Thermo Fisher Scientific) under the following conditions: initial denaturation at 95°C for 7 min, 40 cycles of 95°C for 10 s, 60°C for 30 s, melting curve analysis at 60°C for 30 s. Reactions were performed in triplicate. Sequences for the primers used are given in Table III. Relative quantitation was achieved using the comparative threshold ($\Delta\Delta Ct$) method. mRNA expression levels of target genes in RSA59 infected CD4^{+/+} and CD4^{-/-} mice were normalized with β -Actin and expressed as relative fold change compared to their respective mock-infected controls.

Ultra-structural studies and electron microscopy to characterize the preservation of myelin and axons

To characterize axonal blebbing, disruption of the myelin sheath, and axon-myelin coherence, ultrastructural studies were carried out on the brains, brainstem and spinal cords of mice. Infected CD4^{-/-}, CD4^{+/+} and CD4^{-/-} mock-infected mice were anesthetized and sacrificed at day 28 p.i. Mice were perfused with 4% PFA. Brains and spinal cords were harvested and fixed overnight in 2% glutaraldehyde, post-fixed with 1% osmium tetroxide, and dehydrated in a graded series of ethanol washes. For transmission electron microscopy, samples were flat embedded in Poly-Bed 812 epoxy resin (Polysciences) and sectioned (500 nm) from the lesional epicenter. Toluidine blue staining was performed for examination by light microscopy. Ultrathin TEM sections (600 Å) were trimmed from the representative foci of interest from toluidine blue-stained sections and mounted on 200 mesh copper grids, stained with uranyl acetate and bismuth subnitrate, and viewed under a JEOL JEM 1010 electron microscope (40).

Statistical Analyses

The viral titer was calculated as plaque-forming units (PFU) based on the following formula = (no. of plaques X dilution factor/ml/gram of tissue). Virus titer was expressed as log₁₀

PFU/gram of tissue. Quantitative RT-PCR data were presented as mean values \pm SEM. Values were subjected to Two-Way ANOVA/Student's t-test analysis for calculating the significance of differences between the means. Also, multiple comparisons were achieved by the Tukey test and the Holm-Sidak test. All statistical analyses were done using GraphPad Prism 6 (La Jolla, CA). A P-value of <0.05 was considered statistically significant.

ACKNOWLEDGEMENTS

This work was supported by the Department of Biotechnology [BT/PR 20922/MED/122/37/2016] research grant, India; Animal facility, University of Pennsylvania; Histopathology core, Thomas Jefferson University, Philadelphia, USA; NIH grant EY015014; Research to Prevent Blindness; and the F. M. Kirby Foundation. We thank IISER-Kolkata animal facility for providing necessary support. We thank Ministry of Human Resource Development (MHRD), India, Council of Scientific and Industrial Research (CSIR), India and University Grants Commission (UGC), India for fellowships to DC, FS, AB and SK.

DECLARATIONS

Ethics approval

All experimental procedures and animal care and use were strictly regulated and reviewed in accordance with good animal ethics approved by the Institutional Animal Care and Use Committee at the Indian Institute of Science Education and Research Kolkata (AUP No. IISERK/IAEC/AP/2017/15) and the University of Pennsylvania, Philadelphia, USA (IACUC Protocol No. 804701). Experiments were performed following the guidelines of the Committee for the Purpose of Control and Supervision of Experiments on Animals (CPCSEA), India and the United States National Institutes of Health Office of Laboratory Animal Welfare Guide for the Care and Use of Laboratory Animals, 8th Edition.

Consent for publication

Not Applicable

Availability of data and materials

The datasets used and/or analyzed during the current study will be made available from the corresponding author on reasonable request.

Author Contribution

DC, FD and JDS designed and planned all the experiments. DC, and FS performed the experiments. DC, FS, and JDS analyzed the data and wrote the manuscript. AB, SK, RK and KD helped with the standardization of RNA experiments in the knockout mice. LK blindly read the pathological samples. JDS, KS and LK participated in data analysis and data interpretation. LK and KS were involved in critical revisions of the manuscript. JDS and KS jointly supervised and reviewed this work.

Competing interests

The authors declare that they have no competing interests.

REFERENCES

1. Glass CK, Saijo K, Winner B, Marchetto MC, Gage FH. 2010. Mechanisms Underlying Inflammation in Neurodegeneration. *Cell* 140:918-934.
2. Waisman A, Liblau RS, Becher B. 2015. Innate and adaptive immune responses in the CNS. *The Lancet Neurology* 14:945-955.
3. Prinz M, Priller J. 2017. The role of peripheral immune cells in the CNS in steady state and disease. *Nature Neuroscience* 20:136-144.
4. Schettters STT, Gomez-Nicola D, Garcia-Vallejo JJ, Van Kooyk Y. 2018. Neuroinflammation: Microglia and T Cells Get Ready to Tango. *Frontiers in immunology* 8:1905-1905.
5. McFarlin DE, McFarland HF. 1982. Multiple sclerosis (second of two parts). *The New England journal of medicine* 307:1246-1251.
6. McFarlin DE, McFarland HF. 1982. Multiple sclerosis (first of two parts). *The New England journal of medicine* 307:1183-1188.
7. Zhang J, Markovic-Plese S, Lacet B, Raus J, Weiner HL, Hafler DA. 1994. Increased frequency of interleukin 2-responsive T cells specific for myelin basic protein and proteolipid protein in peripheral blood and cerebrospinal fluid of patients with multiple sclerosis. *The Journal of experimental medicine* 179:973-984.
8. Martin R, McFarland HF. 1995. Immunological aspects of experimental allergic encephalomyelitis and multiple sclerosis. *Critical reviews in clinical laboratory sciences* 32:121-182.
9. Steinman L. 1996. Multiple sclerosis: a coordinated immunological attack against myelin in the central nervous system. *Cell* 85:299-302.
10. Sospedra M, Martin R. 2005. Immunology of multiple sclerosis. *Annual review of immunology* 23:683-747.
11. Kuchroo VK, Anderson AC, Waldner H, Munder M, Bettelli E, Nicholson LB. 2002. T cell response in experimental autoimmune encephalomyelitis (EAE): role of self and cross-reactive antigens in shaping, tuning, and regulating the autopathogenic T cell repertoire. *Annual review of immunology* 20:101-123.
12. Langrish CL, Chen Y, Blumenschein WM, Mattson J, Basham B, Sedgwick JD, McClanahan T, Kastelein RA, Cua DJ. 2005. IL-23 drives a pathogenic T cell population that induces autoimmune inflammation. *The Journal of experimental medicine* 201:233-240.

- 594 13. Martin B, Hirota K, Cua DJ, Stockinger B, Veldhoen M. 2009. Interleukin-17-producing
595 gammadelta T cells selectively expand in response to pathogen products and environmental
596 signals. *Immunity* 31:321-330.
- 597 14. Reboldi A, Coisne C, Baumjohann D, Benvenuto F, Bottinelli D, Lira S, Uccelli A, Lanzavecchia
598 A, Engelhardt B, Sallusto F. 2009. C-C chemokine receptor 6-regulated entry of TH-17 cells into
599 the CNS through the choroid plexus is required for the initiation of EAE. *Nature immunology*
600 10:514-523.
- 601 15. Das Sarma J, Ciric B, Marek R, Sadhukhan S, Caruso ML, Shafagh J, Fitzgerald DC, Shindler KS,
602 Rostami A. 2009. Functional interleukin-17 receptor A is expressed in central nervous system
603 glia and upregulated in experimental autoimmune encephalomyelitis. *Journal of*
604 *neuroinflammation* 6:14-14.
- 605 16. Murphy AC, Lalor SJ, Lynch MA, Mills KHG. 2010. Infiltration of Th1 and Th17 cells and
606 activation of microglia in the CNS during the course of experimental autoimmune
607 encephalomyelitis. *Brain, Behavior, and Immunity* 24:641-651.
- 608 17. Li J, Zhao X, Hao H-W, Shaw MK, Tse HY. 2011. T cells that trigger acute experimental
609 autoimmune encephalomyelitis also mediate subsequent disease relapses and predominantly
610 produce IL-17. *Journal of neuroimmunology* 230:26-32.
- 611 18. Rostami A, Ciric B. 2013. Role of Th17 cells in the pathogenesis of CNS inflammatory
612 demyelination. *Journal of the neurological sciences* 333:76-87.
- 613 19. Hirota K, Duarte JH, Veldhoen M, Hornsby E, Li Y, Cua DJ, Ahlfors H, Wilhelm C, Tolaini M,
614 Menzel U, Garefalaki A, Potocnik AJ, Stockinger B. 2011. Fate mapping of IL-17-producing T
615 cells in inflammatory responses. *Nature immunology* 12:255-263.
- 616 20. Huseby ES, Liggitt D, Brabb T, Schnabel B, Ohlén C, Goverman J. 2001. A pathogenic role for
617 myelin-specific CD8(+) T cells in a model for multiple sclerosis. *The Journal of experimental*
618 *medicine* 194:669-676.
- 619 21. Sun D, Whitaker JN, Huang Z, Liu D, Coleclough C, Wekerle H, Raine CS. 2001. Myelin antigen-
620 specific CD8+ T cells are encephalitogenic and produce severe disease in C57BL/6 mice.
621 *Journal of immunology (Baltimore, Md : 1950)* 166:7579-7587.
- 622 22. Wagner CA, Roqué PJ, Mileur TR, Liggitt D, Goverman JM. 2020. Myelin-specific CD8+ T cells
623 exacerbate brain inflammation in CNS autoimmunity. *The Journal of clinical investigation*
624 130:203-213.
- 625 23. Lane TE, Liu MT, Chen BP, Asensio VC, Samawi RM, Paoletti AD, Campbell IL, Kunkel SL, Fox
626 HS, Buchmeier MJ. 2000. A central role for CD4(+) T cells and RANTES in virus-induced central
627 nervous system inflammation and demyelination. *Journal of virology* 74:1415-1424.
- 628 24. Wu GF, Dandekar AA, Pewe L, Perlman S. 2000. CD4 and CD8 T cells have redundant but not
629 identical roles in virus-induced demyelination. *Journal of immunology (Baltimore, Md : 1950)*
630 165:2278-2286.
- 631 25. Gagliano SA, Pouget JG, Hardy J, Knight J, Barnes MR, Ryten M, Weale ME. 2016. Genomics
632 implicates adaptive and innate immunity in Alzheimer's and Parkinson's diseases. *Annals of*
633 *clinical and translational neurology* 3:924-933.
- 634 26. González H, Pacheco R. 2014. T-cell-mediated regulation of neuroinflammation involved in
635 neurodegenerative diseases. *Journal of neuroinflammation* 11:201-201.
- 636 27. Browne TC, McQuillan K, McManus RM, O'Reilly J-A, Mills KHG, Lynch MA. 2013. IFN- γ
637 Production by amyloid β -specific Th1 cells promotes microglial activation and increases plaque
638 burden in a mouse model of Alzheimer's disease. *Journal of immunology (Baltimore, Md : 1950)*
639 190:2241-2251.
- 640 28. Zhang J, Ke K-F, Liu Z, Qiu Y-H, Peng Y-P. 2013. Th17 cell-mediated neuroinflammation is
641 involved in neurodegeneration of $\alpha\beta 1$ -42-induced Alzheimer's disease model rats. *PloS one*
642 8:e75786-e75786.
- 643 29. Saresella M, Piancone F, Tortorella P, Marventano I, Gatti A, Caputo D, Lunetta C, Corbo M,
644 Rovaris M, Clerici M. 2013. T helper-17 activation dominates the immunologic milieu of both

- amyotrophic lateral sclerosis and progressive multiple sclerosis. *Clinical immunology (Orlando, Fla)* 148:79-88.
30. Brochard V, Combadière B, Prigent A, Laouar Y, Perrin A, Beray-Berthet V, Bonduelle O, Alvarez-Fischer D, Callebort J, Launay J-M, Duyckaerts C, Flavell RA, Hirsch EC, Hunot S. 2009. Infiltration of CD4+ lymphocytes into the brain contributes to neurodegeneration in a mouse model of Parkinson disease. *The Journal of clinical investigation* 119:182-192.
 31. Beers DR, Henkel JS, Zhao W, Wang J, Appel SH. 2008. CD4+ T cells support glial neuroprotection, slow disease progression, and modify glial morphology in an animal model of inherited ALS. *Proceedings of the National Academy of Sciences of the United States of America* 105:15558-15563.
 32. Zheng C, Zhou X-W, Wang J-Z. 2016. The dual roles of cytokines in Alzheimer's disease: update on interleukins, TNF- α , TGF- β and IFN- γ . *Translational neurodegeneration* 5:7-7.
 33. Stohlman SA, Hinton DR, Parra B, Atkinson R, Bergmann CC. 2008. CD4 T Cells Contribute to Virus Control and Pathology following Central Nervous System Infection with Neurotropic Mouse Hepatitis Virus. *Journal of Virology* 82:2130-2139.
 34. Murray PD, Pavelko KD, Leibowitz J, Lin X, Rodriguez M. 1998. CD4(+) and CD8(+) T cells make discrete contributions to demyelination and neurologic disease in a viral model of multiple sclerosis. *Journal of Virology* 72:7320-7329.
 35. Togo T, Akiyama H, Iseki E, Kondo H, Ikeda K, Kato M, Oda T, Tsuchiya K, Kosaka K. 2002. Occurrence of T cells in the brain of Alzheimer's disease and other neurological diseases. *Journal of neuroimmunology* 124:83-92.
 36. Strachan-Whaley M, Rivest S, Yong VW. 2014. Interactions between microglia and T cells in multiple sclerosis pathobiology. *Journal of interferon & cytokine research : the official journal of the International Society for Interferon and Cytokine Research* 34:615-622.
 37. Garber C, Soung A, Vollmer LL, Kanmogne M, Last A, Brown J, Klein RS. 2019. T cells promote microglia-mediated synaptic elimination and cognitive dysfunction during recovery from neuropathogenic flaviviruses. *Nature Neuroscience* 22:1276-1288.
 38. Lavi E, Gilden DH, Wroblewska Z, Rorke LB, Weiss SR. 1984. Experimental demyelination produced by the A59 strain of mouse hepatitis virus. *Neurology* 34:597-603.
 39. Das Sarma J, Scheen E, Seo S-h, Koval M, Weiss SR. 2002. Enhanced green fluorescent protein expression may be used to monitor murine coronavirus spread in vitro and in the mouse central nervous system. *Journal of NeuroVirology* 8:381-391.
 40. Das Sarma J, Kenyon LC, Hingley ST, Shindler KS. 2009. Mechanisms of Primary Axonal Damage in a Viral Model of Multiple Sclerosis. *The Journal of Neuroscience* 29:10272-10280.
 41. Stohlman SA, Weiner LP. 1981. Chronic central nervous system demyelination in mice after JHM virus infection. *Neurology* 31:38-44.
 42. Sutherland RM, Chua MM, Lavi E, Weiss SR, Paterson Y. 1997. CD4+ and CD8+ T cells are not major effectors of mouse hepatitis virus A59-induced demyelinating disease. *Journal of neurovirology* 3:225-228.
 43. Shindler KS, Kenyon LC, Dutt M, Hingley ST, Das Sarma J. 2008. Experimental optic neuritis induced by a demyelinating strain of mouse hepatitis virus. *Journal of virology* 82:8882-8886.
 44. Houtman JJ, Fleming JO. 1996. Pathogenesis of mouse hepatitis virus-induced demyelination. *Journal of neurovirology* 2:361-376.
 45. Biswas K, Chatterjee D, Addya S, Khan RS, Kenyon LC, Choe A, Cohrs RJ, Shindler KS, Das Sarma J. 2016. Demyelinating strain of mouse hepatitis virus infection bridging innate and adaptive immune response in the induction of demyelination. *Clinical immunology (Orlando, Fla)* 170:9-19.
 46. Chatterjee D, Addya S, Khan RS, Kenyon LC, Choe A, Cohrs RJ, Shindler KS, Sarma JD. 2014. Mouse hepatitis virus infection upregulates genes involved in innate immune responses. *PloS one* 9:e111351-e111351.

- 695 47. Kishore A, Kanaujia A, Nag S, Rostami AM, Kenyon LC, Shindler KS, Das Sarma J. 2013. Different
696 mechanisms of inflammation induced in virus and autoimmune-mediated models of multiple
697 sclerosis in C57BL6 mice. *BioMed research international* 2013:589048-589048.
- 698 48. Singh M, Kishore A, Maity D, Sunanda P, Krishnarjuna B, Vappala S, Raghothama S, Kenyon LC,
699 Pal D, Das Sarma J. 2019. A proline insertion-deletion in the spike glycoprotein fusion peptide
700 of mouse hepatitis virus strongly alters neuropathology. doi:10.1074/jbc.RA118.004418.
- 701 49. Zipp F, Aktas O. 2006. The brain as a target of inflammation: common pathways link
702 inflammatory and neurodegenerative diseases. *Trends in neurosciences* 29:518-527.
- 703 50. Aspelund A, Antila S, Proulx ST, Karlén TV, Karaman S, Detmar M, Wiig H, Alitalo K. 2015. A
704 dural lymphatic vascular system that drains brain interstitial fluid and macromolecules. *The*
705 *Journal of experimental medicine* 212:991-999.
- 706 51. Engelhardt B, Ransohoff RM. 2005. The ins and outs of T-lymphocyte trafficking to the CNS:
707 anatomical sites and molecular mechanisms. *Trends in immunology* 26:485-495.
- 708 52. Louveau A, Smirnov I, Keyes TJ, Eccles JD, Rouhani SJ, Peske JD, Derecki NC, Castle D, Mandell
709 JW, Lee KS, Harris TH, Kipnis J. 2015. Structural and functional features of central nervous
710 system lymphatic vessels. *Nature* 523:337-341.
- 711 53. Kivisäkk P, Mahad DJ, Callahan MK, Trebst C, Tucky B, Wei T, Wu L, Baekkevold ES, Lassmann
712 H, Staugaitis SM, Campbell JJ, Ransohoff RM. 2003. Human cerebrospinal fluid central memory
713 CD4⁺ T cells: evidence for trafficking through choroid plexus and meninges via P-selectin.
714 *Proceedings of the National Academy of Sciences of the United States of America* 100:8389-
715 8394.
- 716 54. Zhang J, Weiner HL, Hafler DA. 1992. Autoreactive T Cells in Multiple Sclerosis. *International*
717 *Reviews of Immunology* 9:183-201.
- 718 55. Raine CS. 1994. The Dale E. McFarlin memorial lecture: The immunology of the multiple
719 sclerosis lesion. *Annals of Neurology* 36:S61-S72.
- 720 56. Kaushansky N, Zhong M-C, Kerlero de Rosbo N, Hoefftberger R, Lassmann H, Ben-Nun A. 2006.
721 Epitope Specificity of Autoreactive T and B Cells Associated with Experimental Autoimmune
722 Encephalomyelitis and Optic Neuritis Induced by Oligodendrocyte-Specific Protein in SJL/J
723 Mice. *The Journal of Immunology* 177:7364.
- 724 57. Kaushansky N, Altmann DM, David CS, Lassmann H, Ben-Nun A. 2012. DQB1*0602 rather than
725 DRB1*1501 confers susceptibility to multiple sclerosis-like disease induced by proteolipid
726 protein (PLP). *Journal of Neuroinflammation* 9:29.
- 727 58. Panitch H, Haley A, Hirsch R, Johnson K. 1987. Exacerbations of Multiple Sclerosis in patients
728 treated with gamma Interferon. *The Lancet* 329:893-895.
- 729 59. Bernard CC. 1976. Experimental autoimmune encephalomyelitis in mice: genetic control of
730 susceptibility. *J Immunogenet* 3:263-74.
- 731 60. Miller SD, Vanderlugt CL, Begolka WS, Pao W, Yauch RL, Neville KL, Katz-Levy Y, Carrizosa A,
732 Kim BS. 1997. Persistent infection with Theiler's virus leads to CNS autoimmunity via epitope
733 spreading. *Nat Med* 3:1133-6.
- 734 61. Shemer A, Erny D, Jung S, Prinz M. 2015. Microglia Plasticity During Health and Disease: An
735 Immunological Perspective. *Trends in Immunology* 36:614-624.
- 736 62. Squarzon P, Thion M, Garel S. 2015. Neuronal and microglial regulators of cortical wiring:
737 usual and novel guideposts. *Frontiers in Neuroscience* 9.
- 738 63. Prinz M, Priller J. 2014. Microglia and brain macrophages in the molecular age: from origin to
739 neuropsychiatric disease. *Nature Reviews Neuroscience* 15:300.
- 740 64. Biber K, Möller T, Boddeke E, Prinz M. 2015. Central nervous system myeloid cells as drug
741 targets: current status and translational challenges. *Nature Reviews Drug Discovery* 15:110.
- 742 65. Liddel SA, Guttenplan KA, Clarke LE, Bennett FC, Bohlen CJ, Schirmer L, Bennett ML, Münch
743 AE, Chung W-S, Peterson TC, Wilton DK, Frouin A, Napier BA, Panicker N, Kumar M, Buckwalter
744 MS, Rowitch DH, Dawson VL, Dawson TM, Stevens B, Barres BA. 2017. Neurotoxic reactive
745 astrocytes are induced by activated microglia. *Nature* 541:481.

66. Anderson MA, Burda JE, Ren Y, Ao Y, O'Shea TM, Kawaguchi R, Coppola G, Khakh BS, Deming TJ, Sofroniew MV. 2016. Astrocyte scar formation aids CNS axon regeneration. *Nature* 532:195-200.
67. Rahemtulla A, Fung-Leung WP, Schilham MW, Kündig TM, Sambhara SR, Narendran A, Arabian A, Wakeham A, Paige CJ, Zinkernagel RM, Miller RG, Mak TM. 1991. Normal development and function of CD8+ cells but markedly decreased helper cell activity in mice lacking CD4. *Nature* 353:180-184.
68. Podbielska M, Banik NL, Kurowska E, Hogan EL. 2013. Myelin recovery in multiple sclerosis: the challenge of remyelination. *Brain sciences* 3:1282-1324.
69. Goodman ZD. 2007. Grading and staging systems for inflammation and fibrosis in chronic liver diseases. *Journal of hepatology* 47:598-607.

FIGURE LEGENDS

Fig. 1. Temporal immune cell kinetics in the brains of RSA59 infected mice. Results from flow cytometric analysis of the migration of inflammatory cells and CNS resident cells from the RSA59 infected mice has been summarized in the schematic diagram. The diagram represents the differential infiltration of total myeloid (neutrophils, macrophage/monocytes and microglia) and lymphoid (CD4, CD8 and NKT) cell populations during days 3, 5, 7, 10, 16 and 30 p.i. Respective peaks show highest infiltration at times post infection. ScaleArbitrary.

Fig. 2. Absence of CD4 causes no significant pathology in the mock infected mice. CD4^{+/+} and CD4^{-/-} mice were infected with with an uninfected cell lysate (PBS+0.075% BSA). 5-micron thick liver,brain and spinal cord sections were stained with H&E and CD45 for routine histopathological studies. No inflammation was observed in CD4^{+/+} and CD4^{-/-} mice tissues. Data are represented from 3 independent biological replicates. Scale bars= 50 microns

Fig.3 Absence of CD4 shows no significant alterations in RSA59 induced Liver pathology. CD4^{+/+} and CD4^{-/-} mice were infected with RSA59 and 5-micron thick liver sections were stained with H&E for routine morphological studies. a) Both CD4^{+/+} and CD4^{-/-} mice showed similar features of necrotic/non-necrotic hepatitis. Hepatic Activity Index was calculated according to Ishak's Score as described in materials and methods and plotted (b). c) The average number of hepatic lesions were counted per section from each mouse, combined results were tabulated. Liver sizes and cross-sectional areas were comparable in both CD4^{+/+} and CD^{-/-} mice. Data are represented from 5 independent biological experiments.

Fig.4 Absence of CD4 demonstrates no significant changes in encephalomyelitis upon RSA59 induced acute infection. a, b) At day 6 p.i., sections of brain (panel a) and spinal cord

(panel b) from CD4^{+/+} mice and CD4^{-/-} mice were stained with H&E and immunohistochemically for LCA (leucocyte common antigen). Boxed areas are shown at higher magnification below the corresponding brain midsagittal sections (panel a) or cross sections of spinal cord (panel b). The arrows in the zoomed sections mark characteristic perivascular cuffing and microglial nodule formation mediated by infiltrating inflammatory cells in the H&E-stained sections which correspond to immunoreactive leukocytes and microglia/macrophages in the CD45 immunohistochemically stained sections. Scale bars of midsagittal brain sections represent 1000 microns whereas they represent 100 microns in the higher magnification images shown below. Scale bars of spinal cord cross sections represent 200 microns whereas they represent 50 microns in the higher magnification images shown below. Quantification of the intensity of staining is plotted in a scatter diagram. Statistical analysis was performed using Student's t-test and Welch correction. Data are represented from 5 independent biological experiments.

Fig.5 Absence of CD4 resulted in a significant reduction of CD11b positive microglia/macrophages in the brain and spinal cords during RSA59 induced acute infection. At day 6 p.i., sections of brain and spinal cord from CD4^{+/+} mice and CD4^{-/-} mice were immunohistochemically stained for CD11b (macrophage/microglia activation marker). Boxed areas are shown at higher magnification below the corresponding brain midsagittal sections (upper panel) or cross sections of spinal cord (lower panel). Arrows mark microglia/macrophages in the in the CD11b immunohistochemically stained sections. Scale bars of midsagittal brain sections represent 500 microns whereas they represent 200 microns in the higher magnification images shown below. Scale bars of spinal cord cross sections represent 500 microns whereas they represent 200 microns in the higher magnification images shown below. Quantification of the intensity of staining is plotted in a scatter diagram. Statistical analysis was performed using Student's t-test and Welch correction. ***p<0.001; ****p<0.0001. Data are represented from 5 independent biological experiments. Error bar represents SEM.

Fig.6 Absence of CD4 results in severe poliomyelitis and dorsal root ganglionic inflammation during acute RSA59 infection. Sections of CD4^{+/+} and CD4^{-/-} mouse spinal cords were stained with H&E and immunohistochemically with anti-CD45. There is increased inflammation of the gray matter (poliomyelitis) and dorsal root ganglia in CD4^{-/-} as compared

to CD4^{+/+} mice. Mock-infected mice showed no inflammation. All scale bars indicate 90µm. N=5.

Fig.7 Absence of CD4 results in reduced viral clearance and altered expression of antiviral effector genes. a) Whole-brain lysates from CD4^{+/+} and CD4^{-/-} mice at days 5, 10 and 15 p.i. were subjected to comparative viral plaque assays on confluent monolayers of L2 cells. Each time point represents the mean titer for three mice. Titers are expressed as log10 PFU per gram of tissue. b) The relative abundance of transcripts corresponding to viral N-gene was compared using qRT-PCR in the CD4^{+/+} and CD4^{-/-} infected mouse brains at days 5, 10 and 15 p.i. c) Anti-N immunohistochemistry revealed the differential in-situ distribution of viral antigen in the representative anatomical regions (between brain stem and deep cerebellar white matter) of mock-infected CD4^{+/+}; and RSA59 infected CD4^{+/+} and CD4^{-/-} mice at days 6 and 30 p.i.. Scale bar 100µm (4X) and 50µm (40X). Relative gene expression of IFN γ (d), CXCL10 (e), TNFα (f) and CCL5 (g) at days 5, 10 and 15 p.i. were analyzed by qRT-PCR and compared between CD4^{+/+} and CD4^{-/-} mice. qRT-PCR results were expressed as fold mean ± SEM. Statistical analysis of the data represented in panels a, b, d, e, f, and g) was calculated using Two-way ANOVA, and multiple comparison was achieved by Hom's Sidak; *p<0.05; **p<0.01; ***p<0.001; ****p<0.0001. Data are represented from 3 independent biological experiments, N=3, 3 technical replicates each.

Fig.8 Absence of CD4 leads to severe chronic inflammatory demyelination and axonal loss. a) Cross-sections of CD4^{+/+} and CD4^{-/-} mouse spinal cords were analyzed for the presence of inflammatory lesions by H&E, demyelination by LFB, and inflammatory cells by anti-CD45 and anti-CD11b (microglia/macrophages) immunohistochemistry. Boxed areas are shown at higher magnification to right of the corresponding spinal cord cross sections. Arrows mark demyelinating plaques on the LFB stained sections, infiltrating inflammatory cells in the H&E stained sections, and immunoreactive leukocytes and microglia/macrophages in the CD45 and CD11b immunohistochemically stained sections respectively. Scale bars of spinal cord cross sections represent 200 microns whereas they represent 50 microns in the higher magnification images. Levels of demyelination and inflammation are plotted in a scatter diagram (b, c, d). Statistical significance was calculated by unpaired Student's t-test and Welch correction. ***p< 0.001; ****p<0.0001). Data are represented from 4-5 independent biological experiments. Error bar represents SEM.

Fig.9 Absence of CD4 causes abnormal bulbar (brainstem) vacuolation and neuronal loss in RSA59 infected brains at day 30 p.i. a) Serial sagittal sections of brains from both CD4^{+/+} and CD4^{-/-} mice were analyzed for inflammation at day 30 p.i. by H&E and immunohistochemically by CD45 and CD11b. Boxed areas are shown at higher magnification below the corresponding brain midsagittal sections. Arrows mark infiltrating inflammatory cells in the H&E stained sections, and immunoreactive leukocytes and microglia/macrophages in the CD45 and CD11b immunohistochemically stained sections respectively. Scale bars of spinal cord cross sections represent 200 microns whereas they represent 50 microns in the higher magnification images. Quantification of inflammation was performed for CD45 (b) and CD11b (c) staining. The level of significance was calculated by unpaired Student's t-test and Welch correction, ****p<0.0001). Error bar represents SEM. Data are represented from 4-5 independent biological experiments.

Fig. 10. Absence of CD4 causes no alteration in the axon-myelin coherence in the brain stem and spinal cord of mock infected mice. Toluidine blue stained sections of glutaraldehyde fixed, epoxy resin embedded sections (500 nm thick) from mock infected CD4^{-/-} mouse brain stem (A, B) and spinal cord (C, D). A. Gray and white matter of brain stem. Arrows mark bundles of intact myelinated fibres. Asterisks mark the neuronal nuclei. Original magnification – 400X. B. Brain stem white matter. Original magnification - 1000X. C. Spinal cord cross section. Original magnification 40X. Posterior columns in boxed area are further magnified in D. Original magnification 1000X. White and gray matter in both the brain stem and spinal cord show no evidence of inflammation, demyelination or cellular injury.

Fig.11 Absence of CD4 results in severe spinal cord axonal injury upon RSA59 infection at the chronic stage. a and b: Toluidine blue-stained sections. a) Posterior columns (200X) and b) (1000X) demonstrate clusters of degenerating axons. Arrows - degenerating axons, asterixes - swollen myelin sheaths. c and d: Corresponding electron microscopy. c) Swollen myelin sheaths with loss of axoplasm (7,500X). d) Cluster of degenerating axons with collapsed myelin sheaths (10,000X). The arrow shows the corresponding area on the toluidine blue-stained section. Scale bar represents 2 microns. Data are represented from 3 independent biological experiments.

Fig.12 qRT-PCR analysis of IL-6, IL-10, CD86, Btk and CD163 reveals an inflammatory state in the brains of RSA59 infected CD4^{-/-} mice. Quantitative PCR analysis of IL-6 (a) IL-10 (b); CD86 (c); Btk (d); CD163 (e) analysis was performed in RSA59 infected CD4^{+/+} and

CD4^{-/-} mouse brains at days 5, 10 and 15. Data are represented from 3 independent biological experiments, N=3, 3 technical replicates each. Statistical analysis was performed by Two-way ANOVA, Hom Sidak's multiple comparison test; **p<0.01; ***p<0.001; ****p<0.0001. Error bar represents SEM.

Table I. Average Inflammation score in RSA59-infected CD4^{+/+} and CD4^{-/-} mouse brain (47)

	No. of mice	No. of sections	% mice with inflammation n	Mean score of Inflammation (mean ± SEM)
Acute phase RSA59 CD4 ^{+/+}	4	08	100 %	1.8±0.322
Chronic phase RSA59 CD4 ^{+/+}	5	10	100 %	1.4±0.163
Acute phase RSA59 CD4 ^{-/-}	4	08	100%	2.0±0.189
Chronic Phase RSA59 CD4 ^{-/-}	4	10	100%	2.5±0.189

Significant difference was observed only at the chronic phase of infection between CD4^{+/+} and CD4^{-/-} brains (***p=0.0004)

Table II. Average Inflammation score in RSA59-infected CD4^{+/+} and CD4^{-/-} mouse spinal cord (47)

	No. of mice	No. of sections	% mice with inflammation n	Mean score of Inflammation (mean ± SEM)
Acute phase RSA59 CD4 ^{+/+}	3*	20	80 %	0.6±0.112
Chronic phase RSA59 CD4 ^{+/+}	5	30	100 %	0.76±0.114
Acute phase RSA59 CD4 ^{-/-}	4	20	100%	1.1±0.143
Chronic Phase RSA59 CD4 ^{-/-}	4	20	100%	1.05±0.05

*1 mouse was an outlier; it did not get infected.

Table III. List of Primers

Gene	Forward 5'-3'	Reverse 5'-3'
CD86	GGCTCAAAACATAAGCCTGA	CCCATGTCCTTGATCTGAAC
CD163	GAGACACACGGAGCCATCAA	TGGACAAACCTTTTACAACCA GG
IFN γ	GTCTCTTCTTGGATATCTGGAG GAACT	GTAGTAATCAGGTGTGATTCA ATGACGC
TNF α	CTGTAGCCCACGTCGTAGC	TTGAGATCCATGCCGTTG
CCl5	CCA ATC TTG CAG TCG TGT TTG T	CAT CTC CAA ATA GTT GAT GTA TTC TTG AAC
CXCL10	GACGGTCCGCTGCAACTG	CTTCCCTATGGCCCTCATTCT
Btk1	ACAGCAGAACACATTGCTCA	GGGAACTCCTCAGGAAACAT
IL12 p40	GGAAGCACGGCAGCAGAATA	AACTTGAGGGAGAAGTAGGAA TGG
IL6	AGTTGCCTTCTTGGGACTGA	TCCACGATTTCACAGAGAAC
IL10	AGTGGAGCAGGTGAAGAGTG	TTCGGGAGAGGTACAAACG
Anti -N	AGGATAGAAGTCTGTTGGCTCA	GAGAGAAGTTAGCAAGGTCCT ACG
GAPDH	GCCCCTTCTGCCGATGC	CTTTCCAGAGGGGCCATCC
B- Actin	CTTCTACAATGAGCTGCGTGTG	GGTCTCAAACATGATCTGG

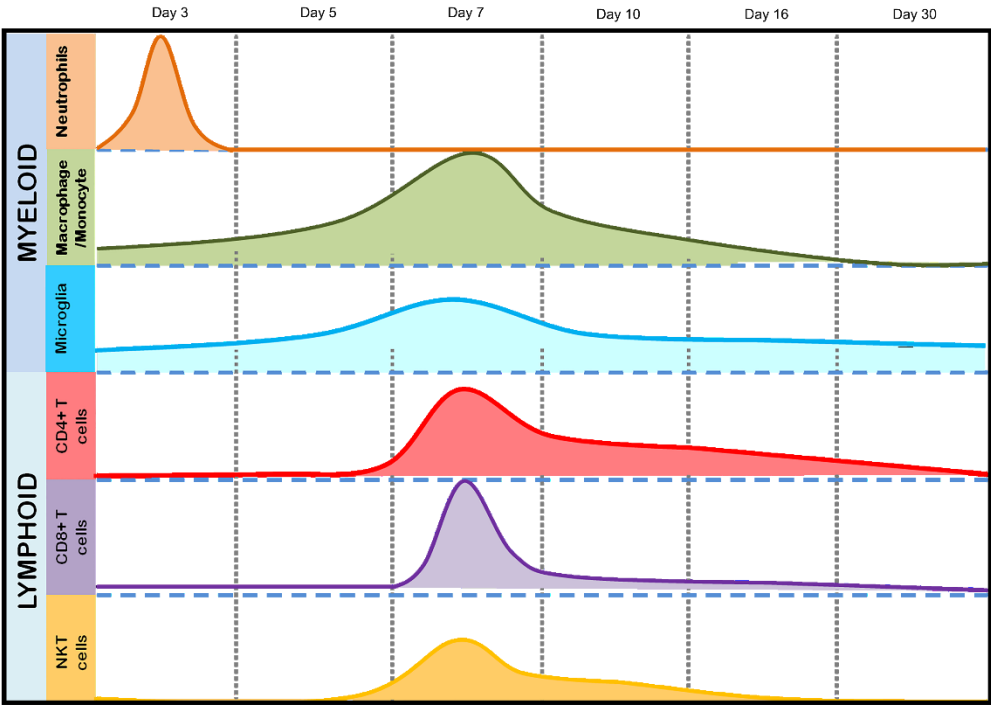
886

887

888

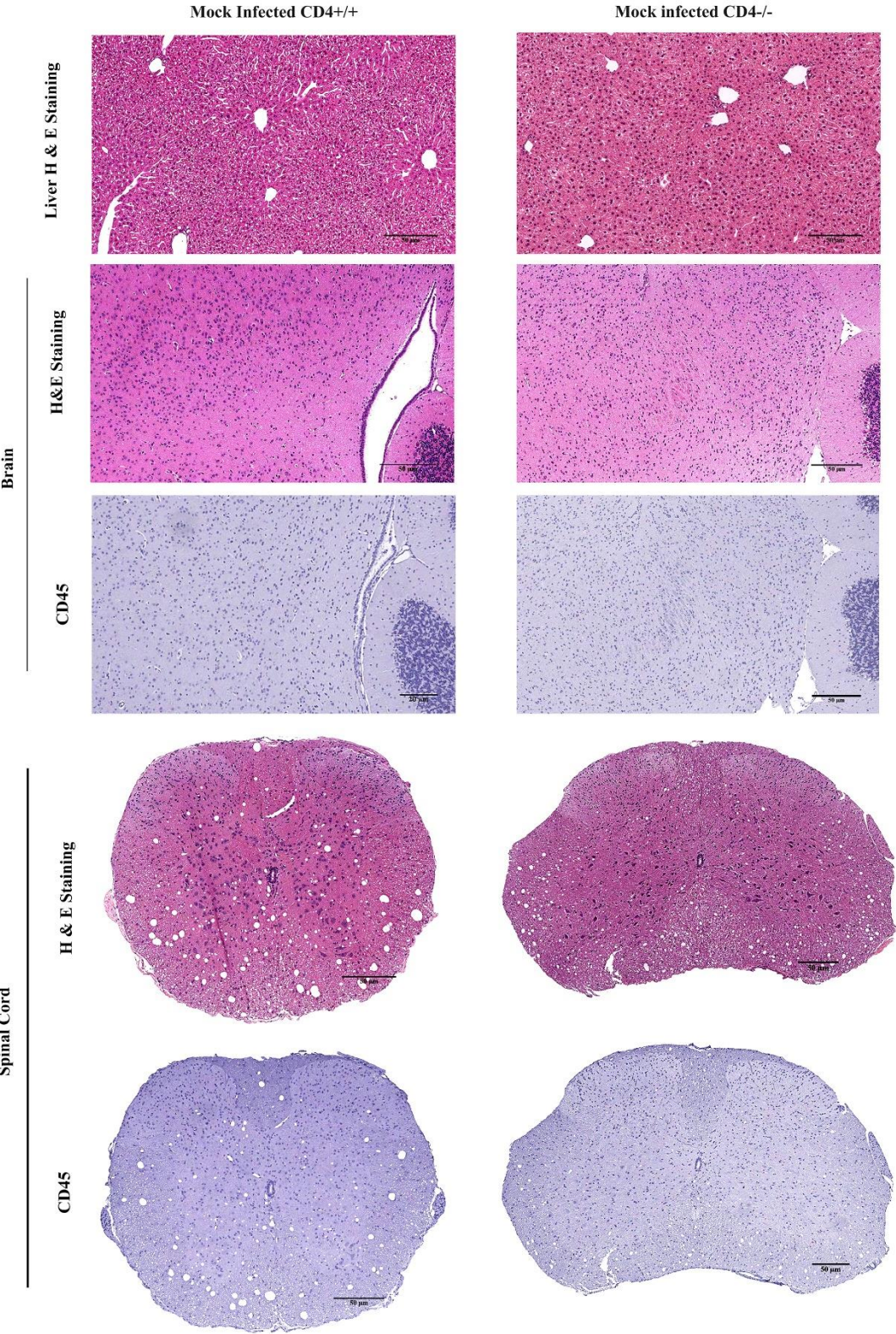
889

Chakravarty et. al., Fig. 1



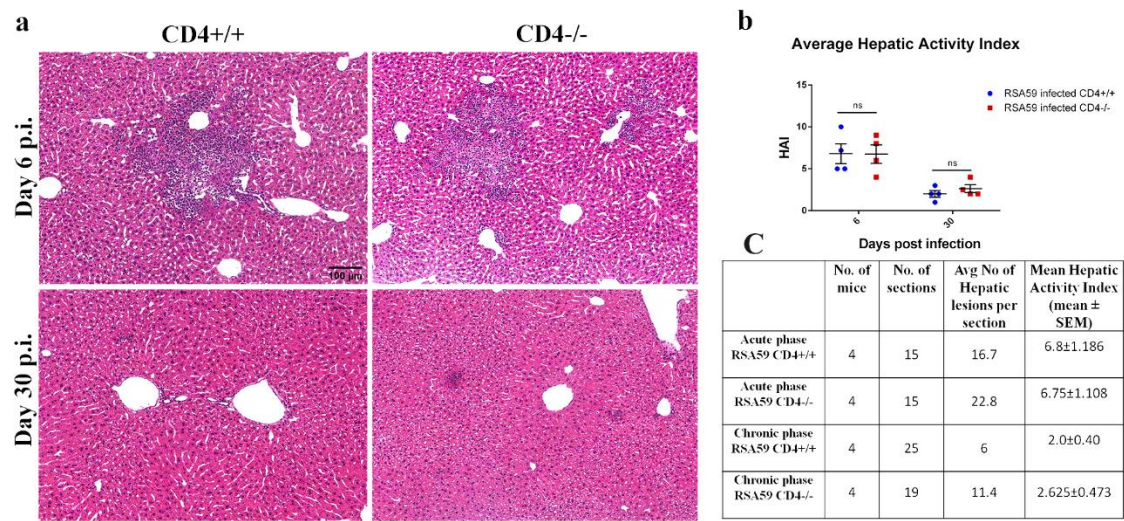
902

903



904

905



906

907

908

909

910

911

912

913

914

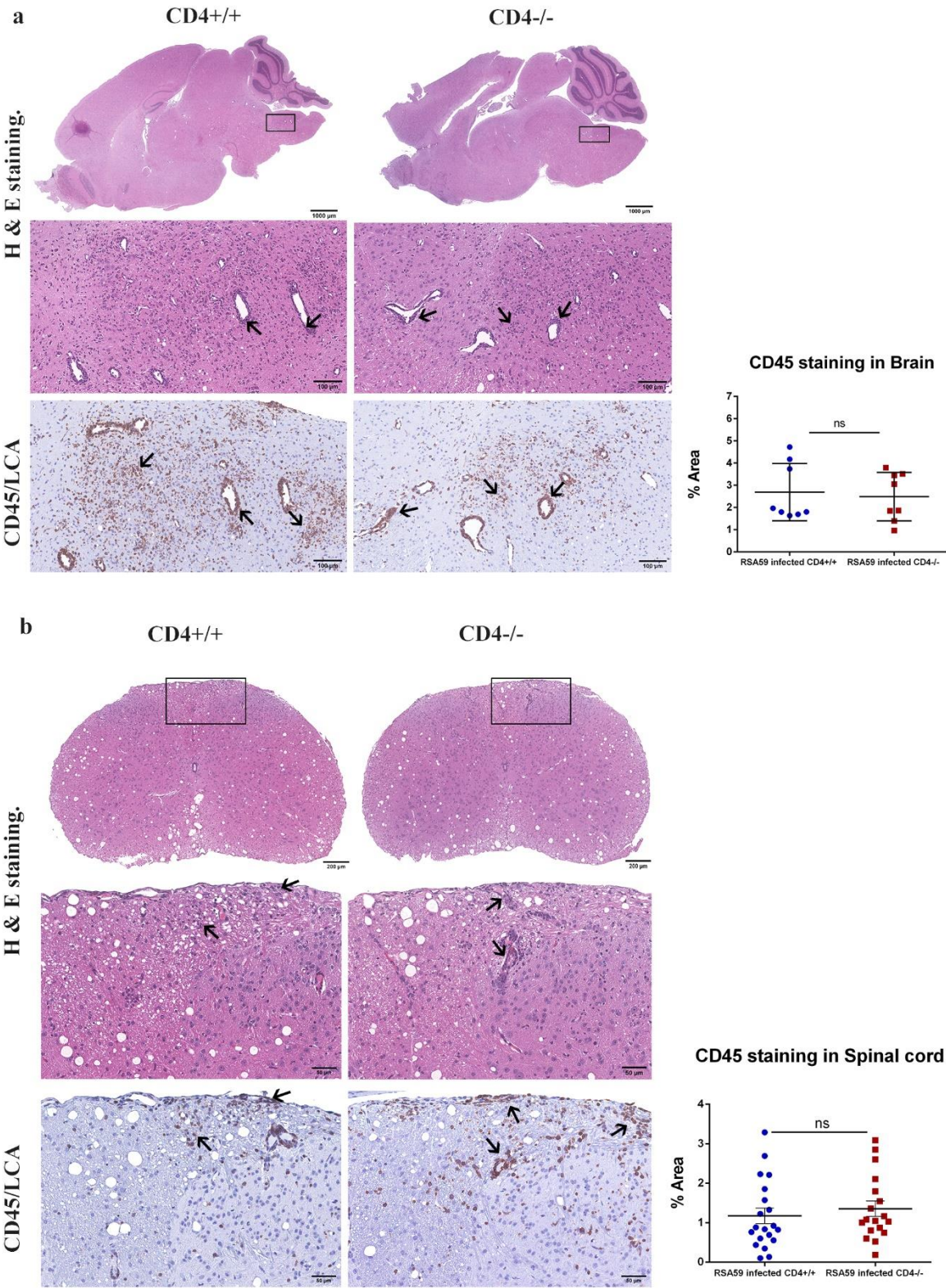
915

916

917

918

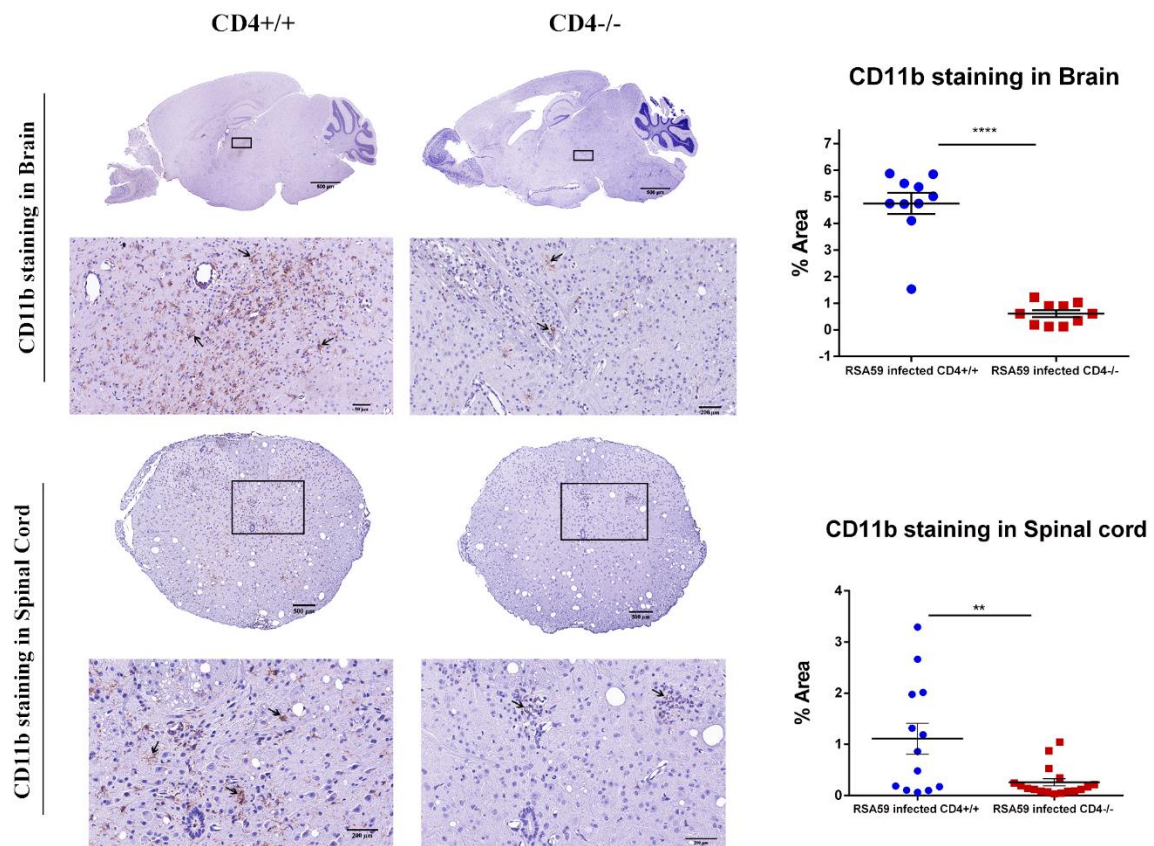
919



920

921

922



923

924

925

926

927

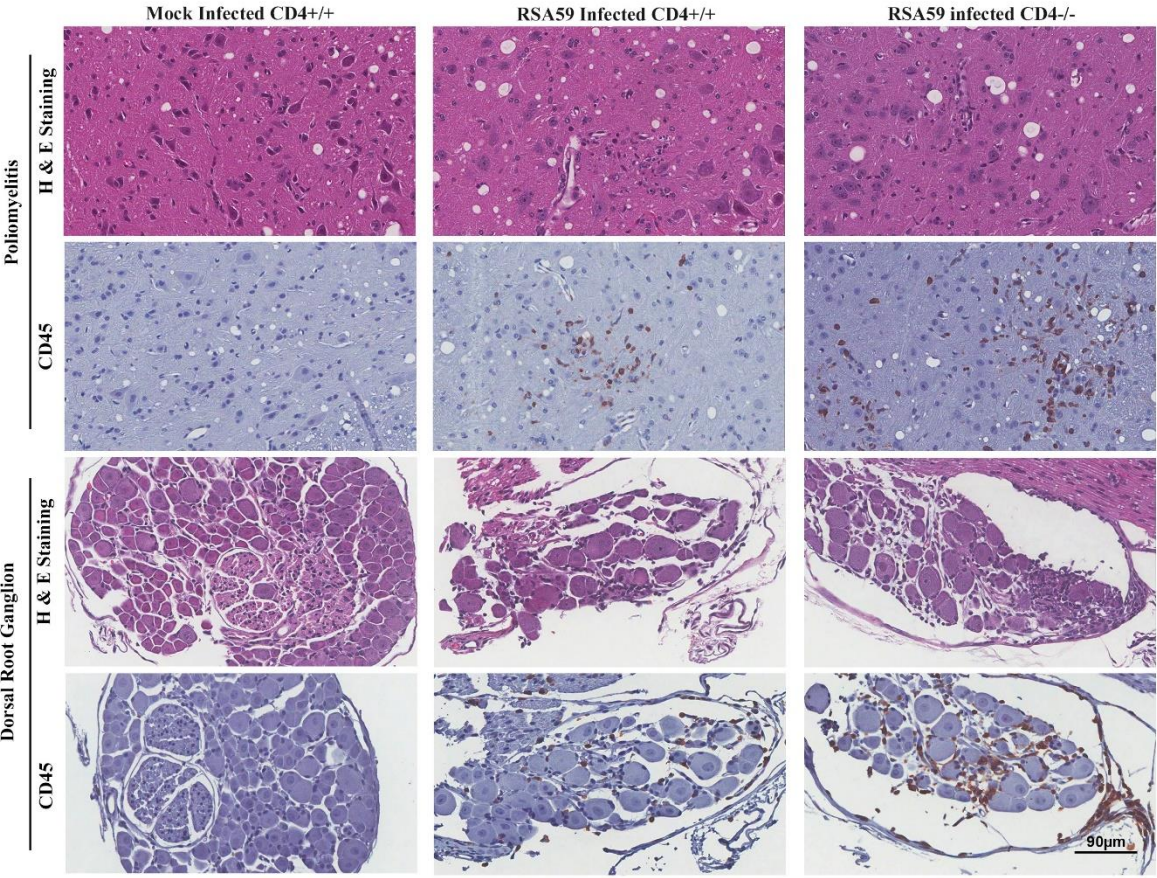
928

929

930

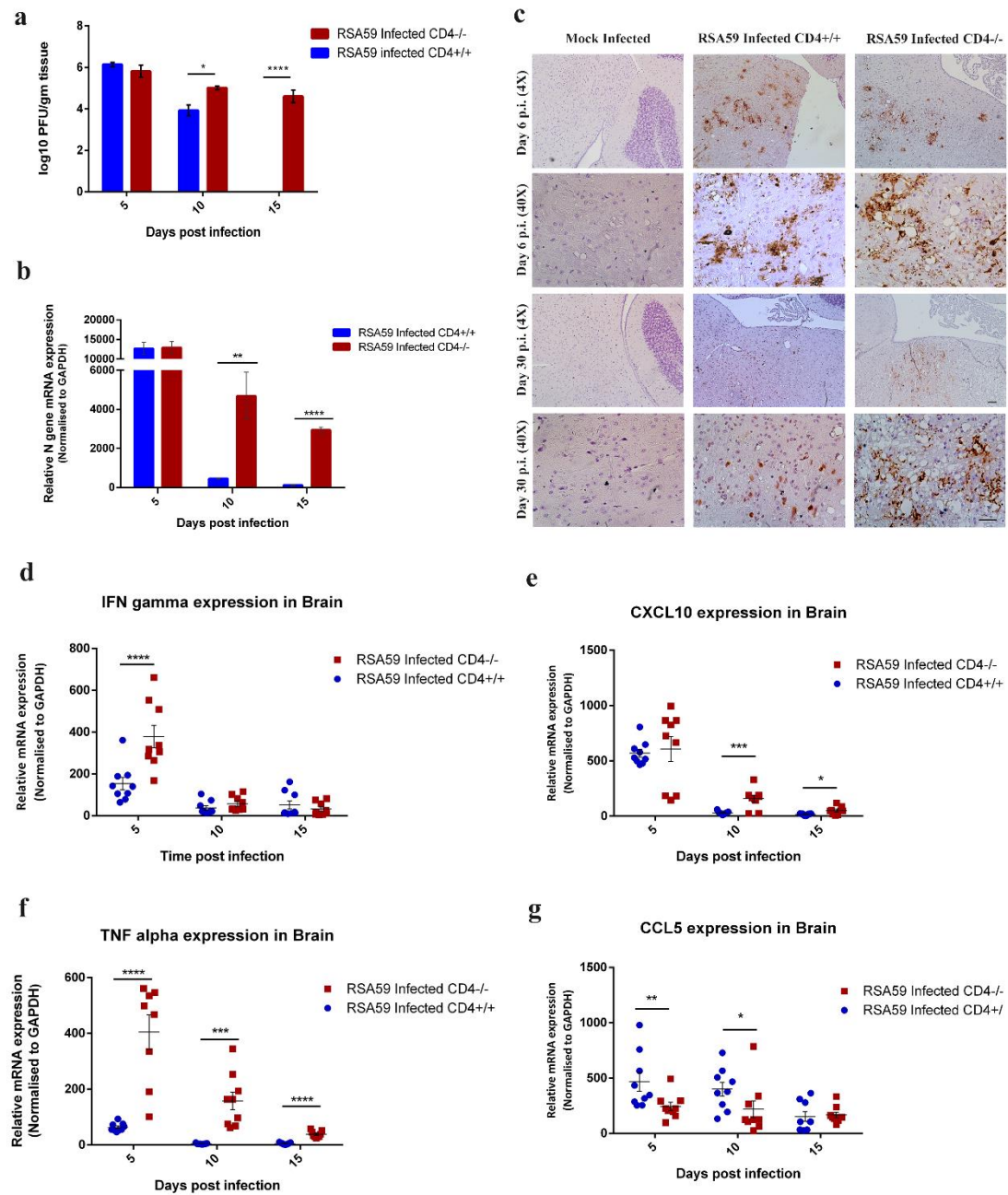
931

Chakravarty et. al., Fig. 6



932
933
934
935
936
937
938
939
940
941

Chakravarty et. al., Fig. 7

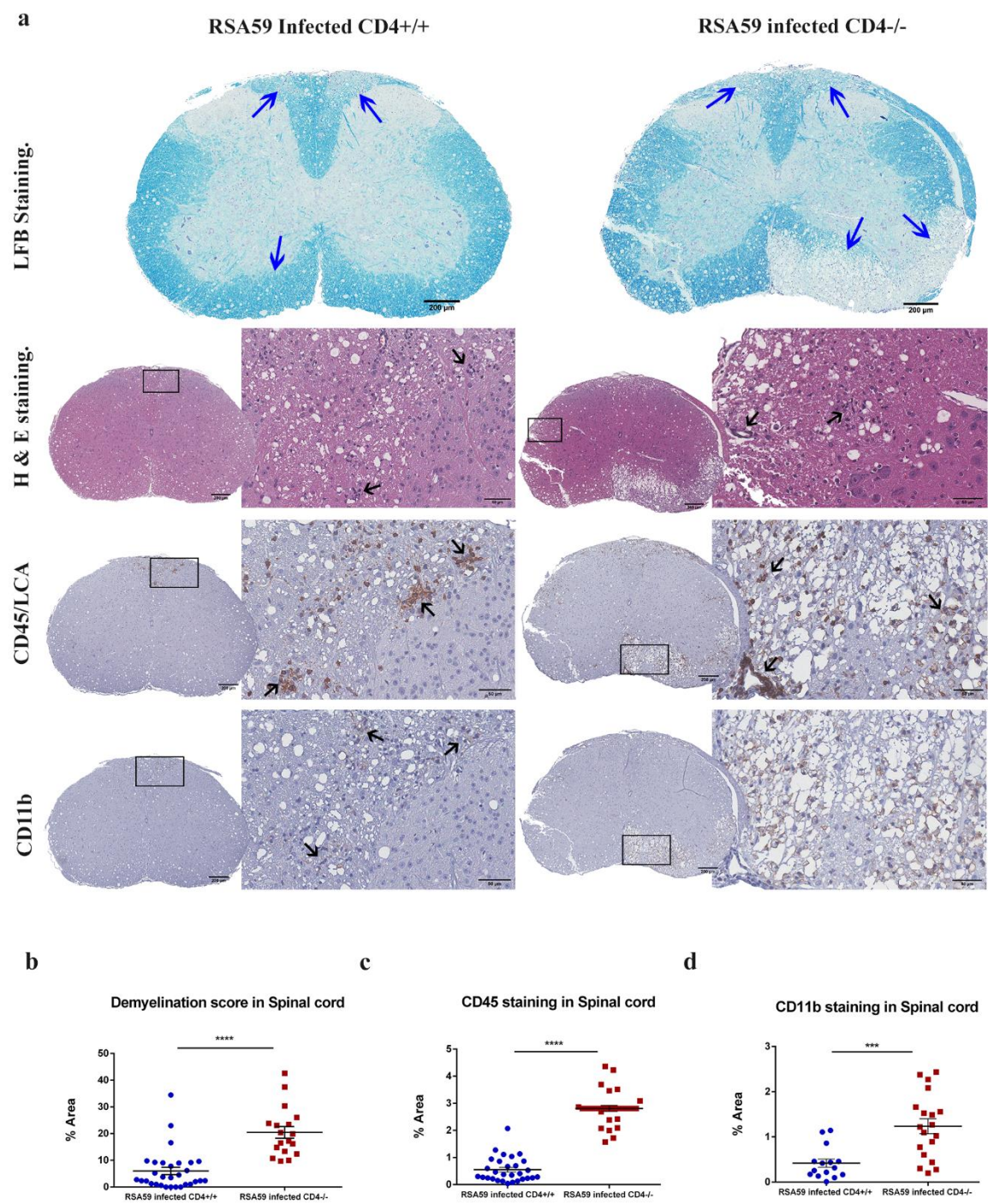


942

943

944

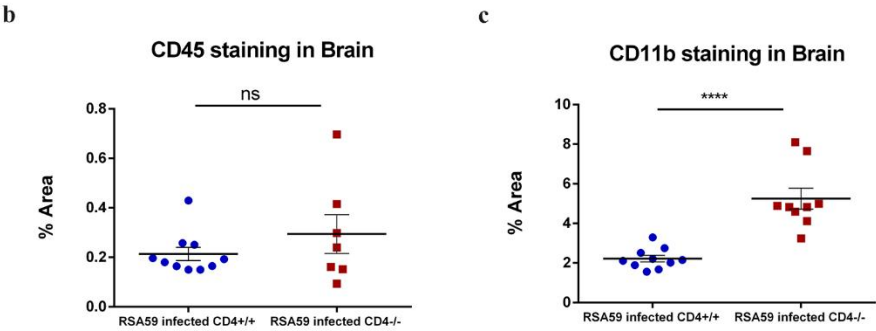
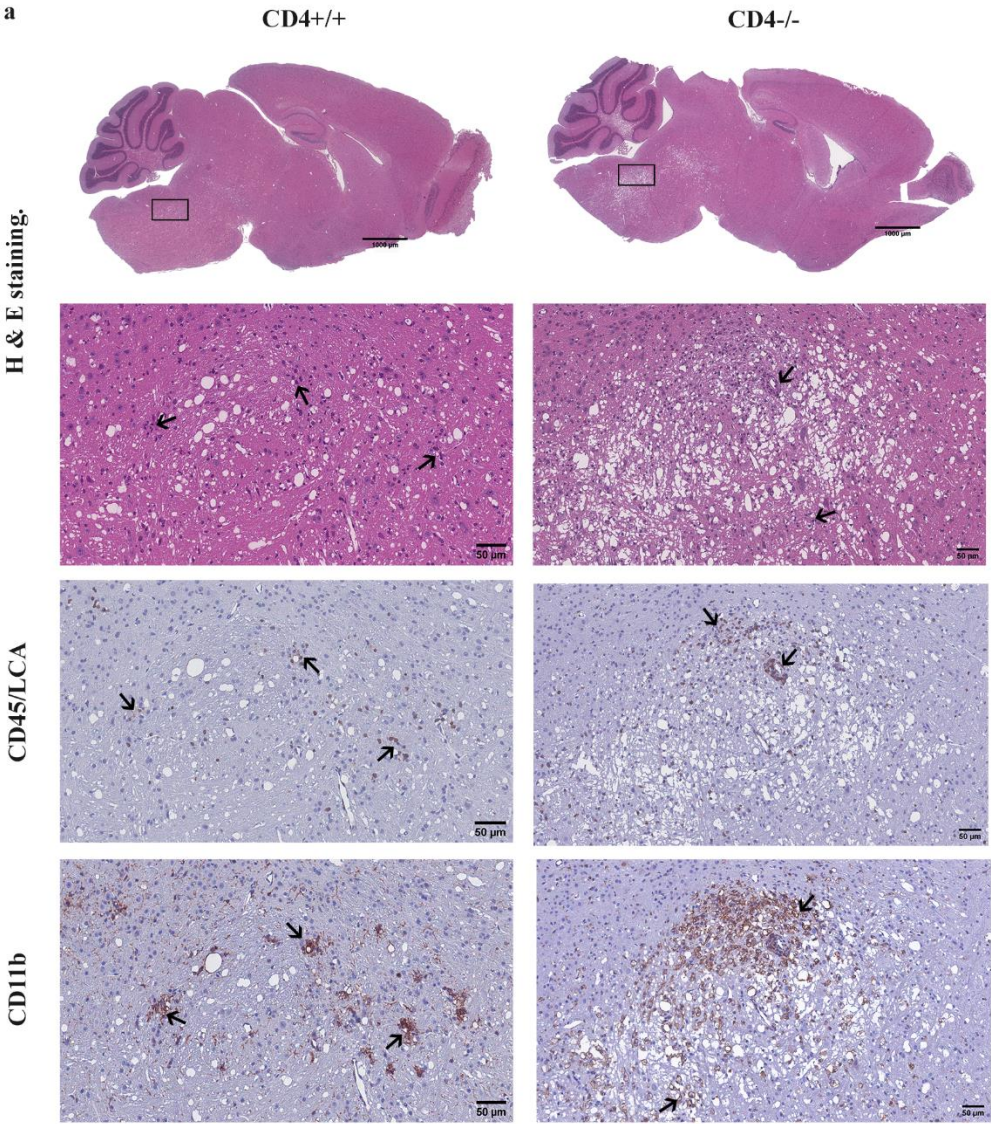
945



946

947

948

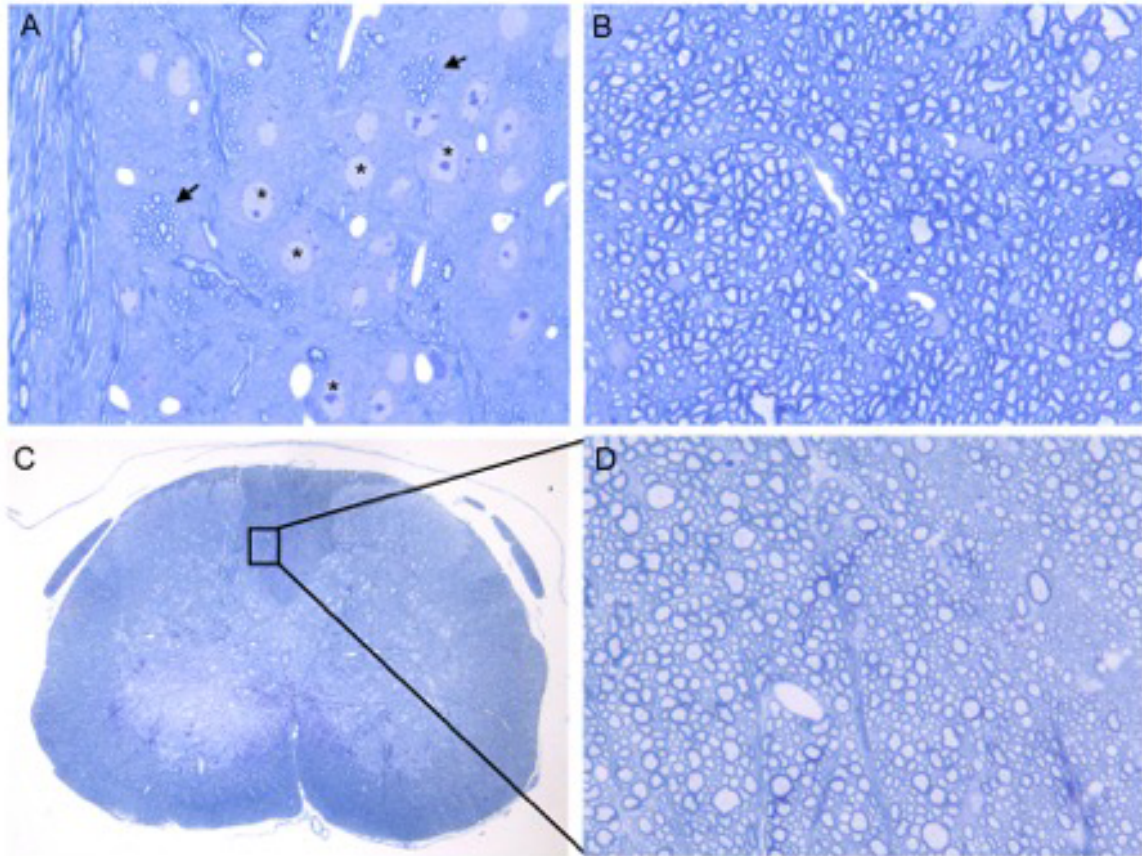


949

950

951

Chakravarty et al., Fig. 10



952

953

954

955

956

957

958

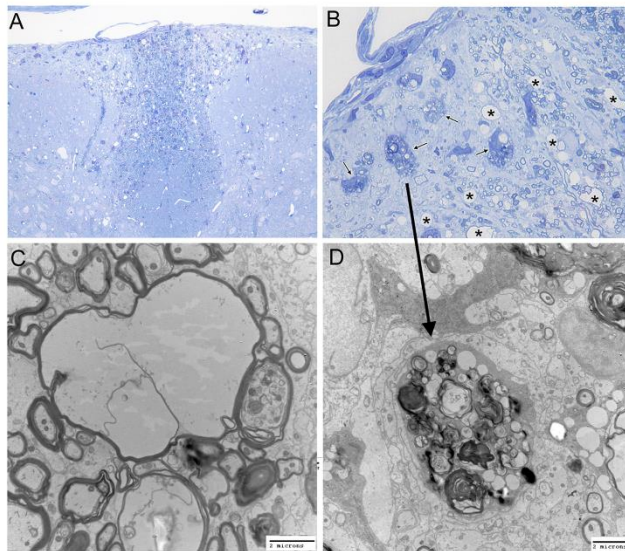
959

960

961

962

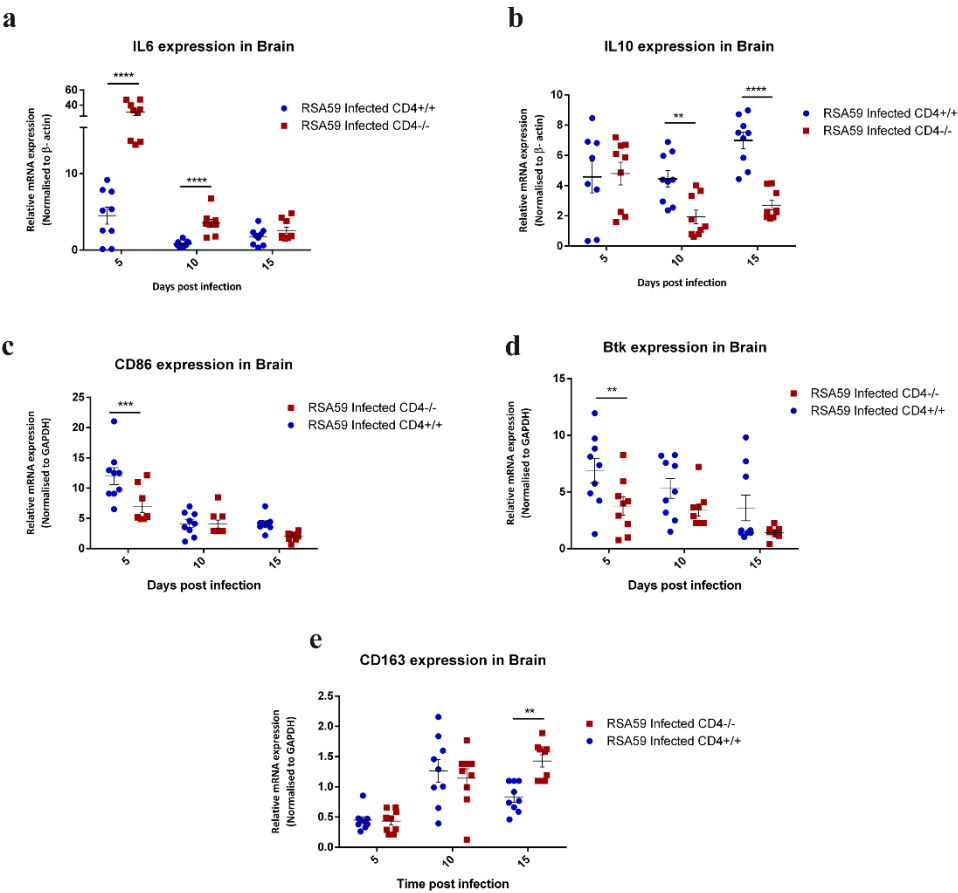
Chakravarty et al., Fig. 11



963

964

965



966

967

968

969

970

971

972

973

974

975

976

977